PHILOSOPHICAL TRANSACTIONS OF THE ROYAL SOCIETY A MATHEMATICAL, PHYSICAL & ENGINEERING SCIENCES

Baroclinic Waves in a Container with Sloping End Walls

P. J. Mason

Phil. Trans. R. Soc. Lond. A 1975 **278**, 397-445
doi: 10.1098/rsta.1975.0032

BAROCLINIC WAVES IN A CONTAINER WITH SLOPING END WALLS

By P. J. MASON
Geophysical Fluid Dynamics Laboratory, Meteorological Office, Bracknell, Berkshire

(*Communicated by R. Hide, F.R.S. – Received 20 August 1974*)

CONTENTS

The effects of sloping upper and lower boundaries on baroclinic waves in a differentially heated rotating fluid annulus have been studied experimentally. Measurements have been made of the internal temperature structure, the transition from axisymmetric to non-axisymmetric flow, the wave numbers and flow types, the drift rates and the heat transfer. The sloping boundaries influence the baroclinic waves in two distinct ways: if they are parallel the energy releasing mechanism is directly affected, while if they are not parallel effects similar to the latitudinal variation of coriolis parameter in a planetary atmosphere (the β-effect) are introduced.

In order to identify essentially non-linear effects the results on the transition from axisymmetric to non-axisymmetric flow, the wave numbers and the drift rates have been compared with an appropriately extended version (by Hide) of Eady's linear perturbation theory of baroclinic instability. In the case of the transition from axisymmetric to non-axisymmetric flow, when account was taken of concomitant changes in the internal temperature structure, surprisingly good agreement with linear theory was obtained. Within the regular wave regime, the azimuthal wave numbers agreed quite well when the theoretically predicted value was 1, 2 or 3 but for higher predicted wave numbers the observed wave numbers were smaller. In the case of oppositely sloping boundaries the observed drift rates relative to the mean flow were generally 30 % less than that of the unstable waves of the linear theory. Another departure from the linear theory also occurred when the boundaries sloped in opposite senses, namely the occurrence at sufficiently rapid rotation rates of *two separate wave trains* of limited radial extent and differing wave numbers and drift speeds; one dominated the flow near the inner cylinder and the other dominated the flow near the outer cylinder. This result suggests that the variation of coriolis parameter with latitude can determine the radial extent of the baroclinic waves.

Apart from its intrinsic interest as a fluid-mechanical study this work bears on the role played by the β-effect and large-scale topography in natural systems such as the atmosphere and oceans. It also shows that at the higher rotation rates used the sloping

geopotentials inevitably present in previous laboratory experiments on baroclinic waves have important effects, and in particular explains the failure of previous theories to account for the position of part of the transition from axisymmetric to non-axisymmetric flow.

1. Introduction

Large-scale waves are observed to play a crucial part in the general circulation of the atmosphere through the potential energy they release and the transports of heat, momentum and other properties they effect. Evidently (Lorenz 1967) these large-scale waves arise from the 'baroclinic instability' of the general circulation. In these 'baroclinic waves' energy is released by the typical trajectories of individual fluid elements which are tilted at an angle to the horizontal that is comparable with but less than the slope of the isotherms. Similar large-scale wave motion is observed in the oceans (Schulman 1967) and may occur in other planetary atmospheres (e.g. Mars (Leovy & Mintz 1969)) and in stellar atmospheres (e.g. the Sun (Ward 1965)).

Thus, a problem of great importance in understanding the circulation of natural fluid systems is the elucidation of the structure of baroclinic waves and the conditions under which they occur.

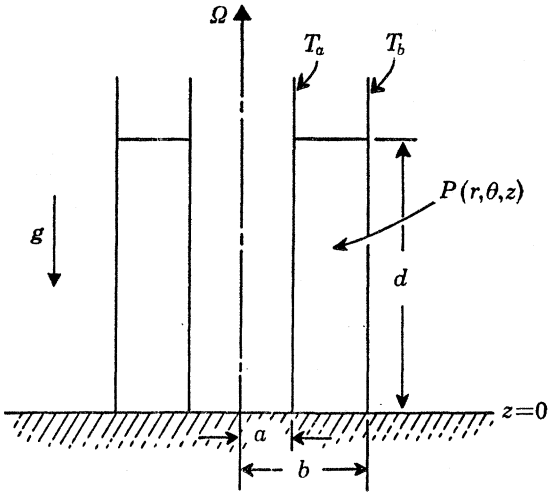

Figure 1. Schematic diagram of the rotating liquid annulus. Cylindrical polar coordinates (r, ϕ, z) of a general point P are fixed in a frame moving with the apparatus, which rotates uniformly with angular velocity Ω about a vertical axis relative to the laboratory (inertial) frame; $\boldsymbol{g} = (0, 0, -g)$ is the acceleration due to gravity. The liquid occupies the region $a < r < b$ and $0 < z < d$. The cylindrical surfaces at $r = a$ and $r = b$ are maintained at constant but different temperatures T_a and T_b respectively.

Theoretical studies of baroclinic instability and baroclinic waves are limited by mathematical difficulties and the speed and size of computing machines, and much of our knowledge of these waves derives from the differentially-heated rotating fluid annulus experiments (see Hide & Mason 1975 for a review). The system investigated in these experiments (see figure 1) is a vertical annulus of liquid bounded by rigid cylindrical surfaces at $r = a$ and $r = b$ (where $b > a$), and by a lower rigid thermally insulating horizontal surface at $z = -\frac{1}{2}d$, the upper surface of the liquid being either a horizontal rigid thermally insulating surface at $z = \frac{1}{2}d$ or a free liquid surface at $(\frac{1}{2}d + \Omega^2[r^2 - \frac{1}{2}(b^2 + a^2)]/2g)$. The two cylindrical surfaces are maintained at constant but different temperatures T_a and T_b, and the whole apparatus rotated about a vertical axis with uniform angular velocity Ω.

Observations of the flow in the annulus over a wide range of experimental conditions has led to the discovery of two distinct classes of flows, i.e. axisymmetric and non-axisymmetric flow (see figures 2 and 3). The non-axisymmetric flow evidently occurs when the axisymmetric flow is baroclinically unstable and three basic forms of fully developed baroclinic waves are observed (figure 2). The first is a 'steady' form in which a wave pattern with a 'wave number' m (number of lobes) simply drifts relative to the rotating apparatus. The second form changes periodically with time, repeating itself at regular intervals (figure 4). This phenomenon has been termed vacillation and in it the waves may change their amplitude, shape, wave number, or a combination

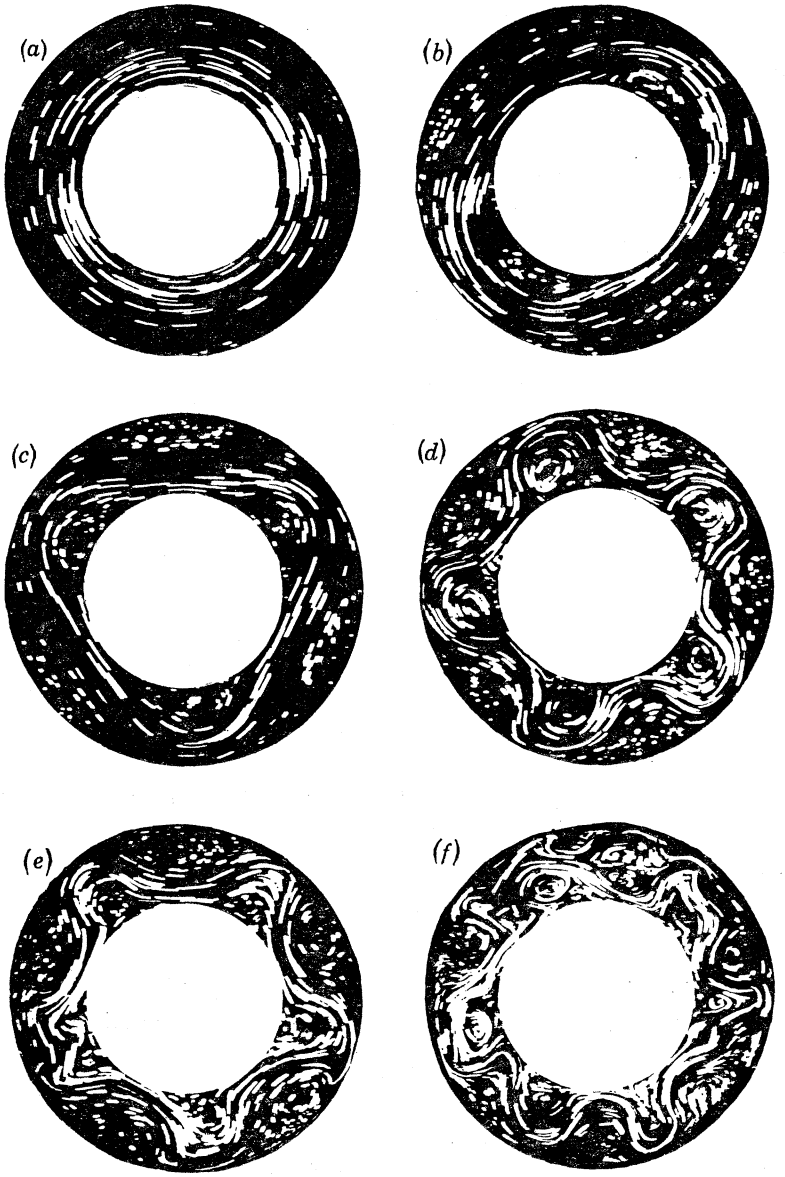

FIGURE 2. Streak photographs illustrating the dependence of the flow type on rotation rate. The values of film exposure duration and angular rotation rate are respectively: (*a*) 1 s, 0.41 rad s^{-1}; (*b*) 1 s, 1.07 rad s^{-1}; (*c*) 1 s, 1.21 rad s^{-1}; (*d*) 2 s, 3.22 rad s^{-1}; (*e*) 2 s, 3.91 rad s^{-1}; (*f*) 3 s, 6.4 rad s^{-1}. Other experimental details: liquid used was water–glycerol solution of mean relative density $\rho = 1.037$ g cm^{-3} and kinematic viscosity $\bar{\nu} = 1.56 \times 10^{-2}$ cm^2 s^{-1}; $T_b - T_a$ was maintained steady to better than 0.5% at values close to 9 K; $b - a = 4.64$ cm, $d = 13.5$ cm; the streak photographs show the flow at a depth of 0.5 cm below the free upper surface.

of these properties. The third form is irregular (figure 5) and appears to be aperiodic although the spatial and temporal spectra characterizing such flows have yet to be measured.

This paper is concerned with the influence on baroclinic instability and fully developed baroclinic waves in such a rotating fluid annulus, of upper and lower boundaries which slope in the radial direction. To assist in understanding the results a detailed comparison with the linear perturbation theory of Hide (1969) has been made. Hide's theory extends Eady's (1949) to include the effects of both Ekman layers (Barcilon 1964) and sloping upper and lower boundaries.

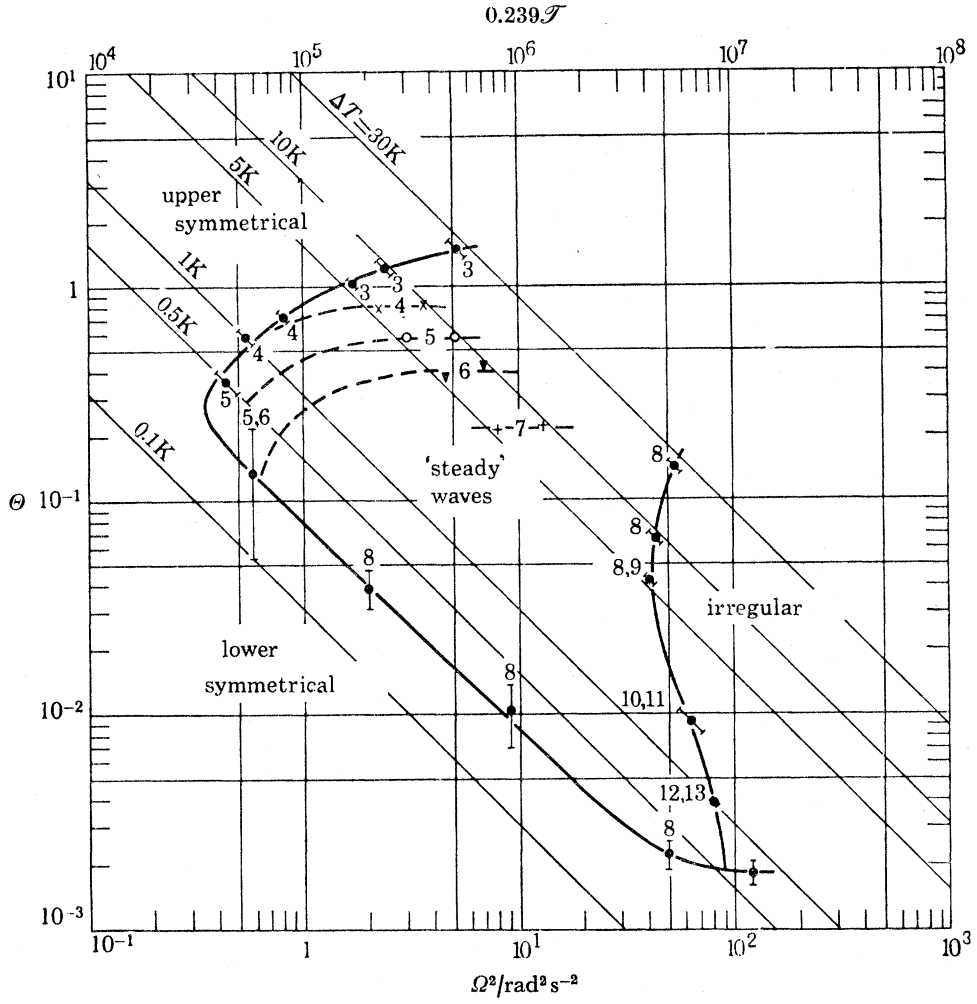

FIGURE 3. Typical régime diagram (after Fowlis & Hide 1965) illustrating the conditions under which axisymmetric flow, steady waves and irregular flow occur,

$$\Theta = g\alpha|T_b - T_a|\, d/\Omega^2(b-a)^2 \quad \text{and} \quad \mathscr{T} = 4\Omega^2(b-a)^5/\bar{\nu}^2 d.$$

Experimental details: working fluid water with the upper surface free; $a = 3.48$ cm, $b = 6.02$ cm, $d = 10.0$ cm, $\bar{\nu} = 1.01 \times 10^{-2}$ cm^2 s^{-1}, $\bar{\rho} = 0.998$ g cm^{-3}.

This comparison is not meant to test or verify the linear theory but to see to what extent it applies to the fully developed waves, thereby assisting in identifying essentially non-linear effects.

In this theory the effect of the slope of the boundaries depends on the ratio of the slope of the boundaries to the slope of the isotherms, i.e. Q_u for the upper boundary and Q_l for the lower boundary. Two distinct types of effect can be produced by sloping the boundaries; if the

boundaries remain parallel to each other ($Q_u = Q_l$) the sloping convection mechanism of the baroclinic instability is directly affected, whereas if the boundaries slope at equal but opposite angles ($Q_u = -Q_l$) effects roughly equivalent to an overall radial vorticity gradient are introduced. In a barotropic fluid vorticity gradients due to the shear of the basic flow or the variation of coriolis parameter with latitude – 'the β-effect' – may be shown to be formally equivalent to a variation of depth of the rotating container. If the boundaries slope in a more general fashion, combinations of these two effects occur.

In the experiments the isotherm slope in the interior of the fluid is determined by the convection so that if the boundaries are sloped the isotherm slope will in general change. When

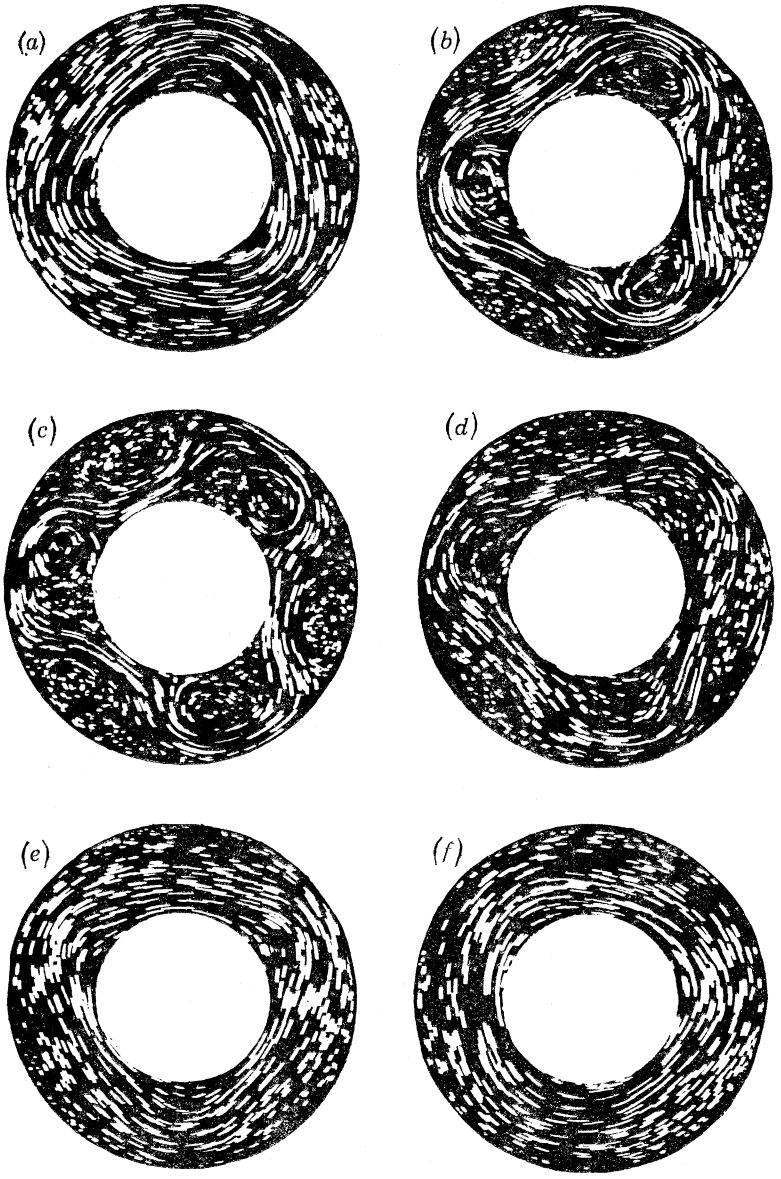

FIGURE 4. Streak photographs illustrating an amplitude 'vacillation'. The time interval between photographs is 30 s and the exposure duration is 2 s. Other experimental details: liquid used was water–glycerol solution of mean density $\bar{\rho} = 1.037\,\mathrm{g\,cm^{-3}}$ and kinematic viscosity $\bar{\nu} = 1.56 \times 10^{-2}\,\mathrm{cm^2\,s^{-1}}$; $T_b - T_a = 8.8\,\mathrm{K}$, $b - a = 4.64\,\mathrm{cm}$; $d = 13.7\,\mathrm{cm}$, $\Omega = 1.1\,\mathrm{rad\,s^{-1}}$; the streak photographs show flow at a depth of 0.5 cm below the rigid upper surface.

account is taken (cf. Fultz & Kaylor 1959) of these concomitant changes in internal temperature structure fairly good agreement with the linear theory is obtained. In particular good agreement is obtained between the parameters for the transition from axisymmetric to non-axisymmetric flow in the experiments and marginal stability in the theory.

When the boundaries slope but remain parallel ($Q_l = Q_u$) the theory indicates large changes in the unstable wave numbers. In spite of these changes the experiments find the relation between the observed wave numbers and the theoretically most unstable wave numbers is independent of the boundary slopes. Near marginal stability the agreement is good but elsewhere the observed wave numbers are smaller than the theoretically most unstable ones. The transition from steady wave flow to irregular flow is strongly affected by the parallel sloping boundaries but the

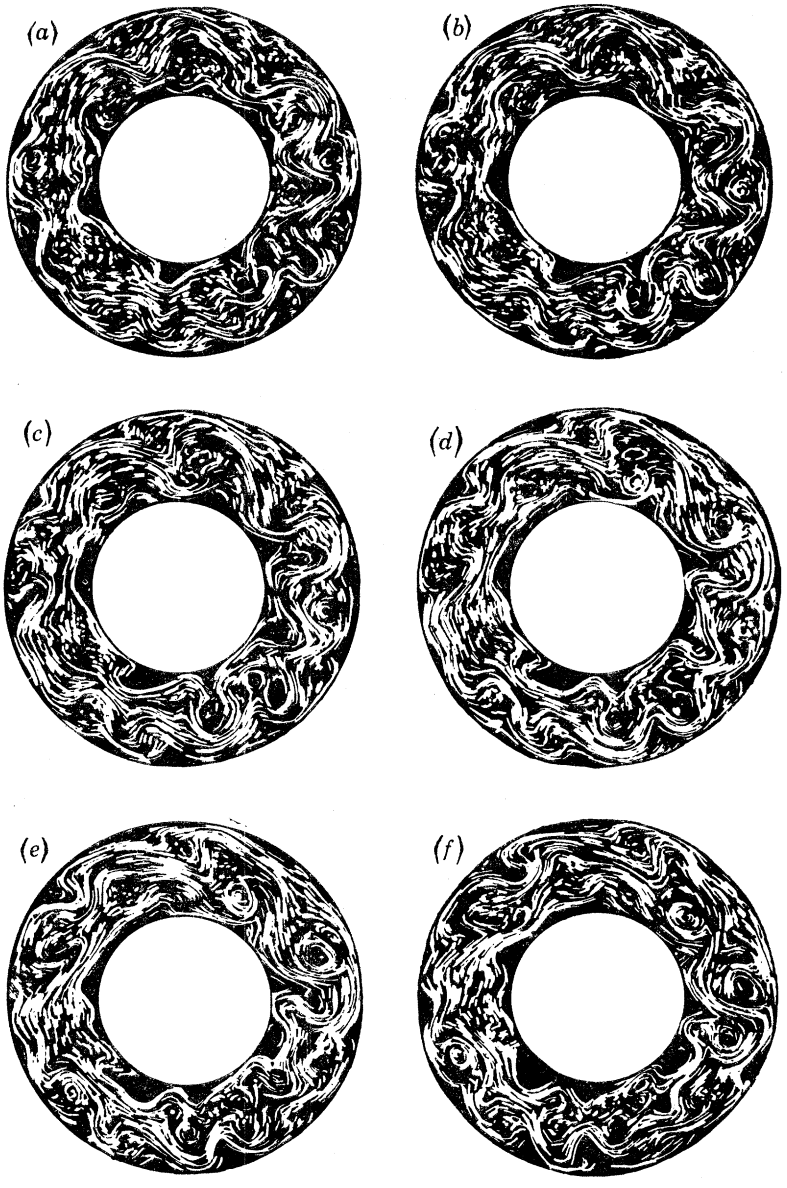

FIGURE 5. Streak photographs illustrating an irregular flow. The time interval between photographs is 5 s and the exposure duration is 2 s. Other experimental details: liquid used water; $\frac{1}{2}(T_b + T_a) = 20.0\,^{\circ}\mathrm{C}$, $T_b - T_a = -9.7\,\mathrm{K}$, $b - a = 4.64\,\mathrm{cm}$, $d = 13.5\,\mathrm{cm}$, $\Omega = 6.0\,\mathrm{rad\,s^{-1}}$; the streak photographs show the motion of aluminium powder floating on the free liquid surface.

PHILOSOPHICAL TRANSACTIONS OF THE ROYAL SOCIETY A MATHEMATICAL, PHYSICAL & ENGINEERING SCIENCES

maximum wave numbers which occur at this transition still agree with the geometrically (Hide 1958) determined value found without sloping boundaries.

In connexion with vacillation it was observed that with slopes that reduced the growth rates in the theory ($Q_1 = Q_u < 0$) vacillation seldom occurred but, when the slopes increased the growth rates ($Q_1 = Q_u > 0$) vacillation frequently occurred. With $Q_1 = -Q_u$ the frequency of vacillation (see § 4 (*c*)) was much as with $Q_1 = Q_u = 0$, but the phenomenon of wave dispersion (see § 4 (*c*)) was much more prevalent than with any of the other types of slope.

The oppositely sloping boundaries ($Q_1 = -Q_u$), like a β-effect, make the waves drift relative to the mean flow. The linear theory gives values of this drift similar to those of a Rossby wave and the values of this drift for the fully developed baroclinic waves in the experiments are between 40 and 80 % of the values given by the linear theory. The oppositely sloping boundaries also introduced a new effect not described by the theory, namely the reduction of the radial scale of the waves to a value less than $(b-a)$. Thus for the larger values of slope and higher rotation rates two separate wave trains of limited radial extent occurred together; one dominating the flow near the inner cylinder and the other dominating the flow near the outer cylinder.

Previous experiments ($Q_1 = Q_u = 0$) found the heat transfer to decrease with increasing Ω in the axisymmetric and irregular régimes but to be roughly constant in the wave régime. The changes in flow types produced by parallel slopes ($Q_1 = Q_u$) were thus accompanied by large changes in heat transfer. The effect of oppositely sloping boundaries ($Q_1 = -Q_u$) was similar except that the heat transfer was found to decrease slightly with increasing Ω in the wave régime.

This study bears on the effect, in natural systems, of topography larger in scale than the baroclinic waves. Such effects have been discussed in relation to the Martian atmosphere by Blumsack & Gierasch (1972) and in relation to the ocean by Orlanski & Cox (1973). The atmosphere is also subject to such effects not only through the topography of the ground but also through the isotherm structure implied by variations in the height of the tropopause (Charney & Stern 1962; Pedlosky 1964). Furthermore these natural systems are subject to the β-effect and the experiments with oppositely sloping boundaries indicate some effects which may be expected.

This study also bears on previous studies of baroclinic waves in a rotating fluid annulus in as much as effects akin to those due to sloping boundaries, but arising from the parabolic slope of the geopotential surfaces, have inevitably been present to some degree. Near the upper symmetric transition (see figure 3) these effects are negligible but at higher rotation rates near the irregular and lower symmetric transition they are significant. In particular it appears (see § 2 (*d*)) that the shape of the lower symmetric transition is strongly affected.

The linear theory and the calculations based on it are presented in § 2. The apparatus and experimental procedure are described in § 3. The experimental results then follow in § 4.

2. Linear stability theory

(*a*) *Basic equations*

It is instructive to outline Hide's (1969) extension of Eady's (1949) theory to include both Ekman layers (following Barcilon 1964) and sloping upper and lower boundaries (see Hide 1969, Appendix C, for details of the analysis) and apply the theory to systems analogous to those investigated in the experimental work described in §§ 3 and 4.

The equations of the problem are:

$$\rho = -\bar{\rho}\alpha(T-\bar{T}), \tag{2.1}$$

$$\partial \boldsymbol{u}/\partial t + (\boldsymbol{u}\cdot\nabla)\,\boldsymbol{u} + 2\boldsymbol{\Omega}\times\boldsymbol{u} = -1/\rho\nabla(p+\bar{p}) - \boldsymbol{g}[(\rho+\bar{\rho})/\bar{\rho}] + \nu\nabla^2\boldsymbol{u}, \tag{2.2}$$

$$\nabla\cdot\boldsymbol{u} = 0, \tag{2.3}$$

$$\partial\rho/\partial t + \boldsymbol{u}\cdot\nabla\rho = \chi\nabla^2\rho \tag{2.4}$$

and

$$\partial\bar{\rho}/\partial z + g\bar{\rho} = 0. \tag{2.5}$$

Curvature of the annular system is neglected and a local cartesian coordinate system related to cylindrical polar coordinates by

$$(x, y, z) = \{\tfrac{1}{2}(b+a)\,\phi,\ -[r-\tfrac{1}{2}(b+a)],\ z\} \tag{2.6}$$

is used. The fluid is bounded by vertical walls at $y = \pm\frac{1}{2}(b+a)$, and there are thin viscous boundary layers whose thickness is neglected on the upper and lower boundaries at $z = z_1(y)$ and $z = z_u(y)$. Both viscosity and thermal conductivity are taken as equal to zero in the interior of the fluid.

The basic density structure is taken as

$$\rho_0 = y\,\partial\rho_0/\partial y + z\,\partial\rho_0/\partial z \tag{2.7}$$

and the basic flow $\boldsymbol{u}_0 = (u_0, v_0, w_0)$ is given by

$$w_0 = v_0 = 0 \tag{2.8}$$

and the 'thermal wind' equation

$$2\Omega\,\partial u_0/\partial z = (g/\rho)\,\partial\rho_0/\partial y. \tag{2.9}$$

The flow is assumed to consist of a small perturbation u_1, to the basic flow u_0, i.e.

$$u = u_0(z) + u_1(x, y, z, t)$$

and terms of the second degree in perturbed quantities are neglected.

The boundary conditions on the radial component of velocity v are

$$v = 0 \quad \text{at} \quad y = \pm\tfrac{1}{2}(b-a). \tag{2.10}$$

The boundary conditions on the vertical component of velocity w, at the lower and upper boundaries

$$z_1 = -\tfrac{1}{2}d + \theta_1 y \tag{2.11}$$

and

$$z_u = \tfrac{1}{2}d + \theta_u y, \tag{2.12}$$

are applied at $z = \pm\frac{1}{2}d$ and are

$$w = \theta_1 v + \frac{1}{2}\left(\frac{\nu}{\Omega}\right)^{\frac{1}{2}}\left(\frac{\partial v}{\partial x} - \frac{\partial u}{\partial y}\right) \quad \text{at} \quad z = -\tfrac{1}{2}d \tag{2.13}$$

and

$$w = \theta_u v - \frac{1}{2}\left(\frac{\nu}{\Omega}\right)^{\frac{1}{2}}\left(\frac{\partial v}{\partial x} - \frac{\partial u}{\partial y}\right) \quad \text{at} \quad z = \tfrac{1}{2}d. \tag{2.14}$$

The equations are scaled with $(b-a)$ for horizontal distance, d for vertical distance, $U_0 \equiv gd(\partial\rho_0/\partial y)/2\Omega\bar{\rho}$ (see equation (2.9)) for horizontal velocity, $U_0 d/(b-a)$ for vertical velocity, $(b-a)/U_0$ for time, $2\Omega U_0\rho(b-a)$ for pressure and $\bar{\rho}(b-a)\,2\Omega U_0/gd$ for density. The dimensionless numbers

$$R \equiv gd(\partial\rho_0/\partial y)/4\Omega^2\bar{\rho}(b-a), \tag{2.15}$$

$$B \equiv -gd^2(\partial\rho_0/\partial z)/4\Omega^2\bar{\rho}(b-a)^2 \tag{2.16}$$

and

$$\mathscr{E} \equiv \tfrac{1}{2}(\nu/\Omega d)^{\frac{1}{2}} \tag{2.17}$$

are introduced. Making use of the assumption that $R \ll 1$ and $B = O(1)$ we can expand the perturbed and scaled variables in a series in powers of the thermal Rossby number R. From this expansion it follows that $w = O(Rud/(b-a))$ and to be consistent this sets limits through equations (2.13) and (2.14) on the size of θ_1, θ_u and $\mathscr{E}$. A partial differential equation for the perturbed and scaled pressure p is then obtained from the first order terms. If solutions are sought of the form

$$P(x, y, z, t) = Z(z)\, e^{ikx - ik\hat{c}t} \cos n\pi y \tag{2.18}$$

where k is real and positive and n is an odd integer, then by using the boundary conditions a quadratic equation for $\hat{c}$, the complex phase speed, is obtained, i.e.

$$\hat{c}^2 + \hat{c}(\coth\gamma/\gamma)\,(2iF + Q_1 + Q_u) - (1/\gamma^2)\{1 + \tfrac{1}{4}\gamma^2 + F^2 - iF(Q_1 - Q_u) - (Q_1 + Q_u) + Q_1 Q_u - \gamma \coth\gamma[1 - \tfrac{1}{2}(Q_1 + Q_u)]\} = 0, \tag{2.19}$$

where

$$\gamma = (B(k^2 + n^2\pi^2))^{\frac{1}{2}}, \tag{2.20}$$

$$F = \mathscr{E}\gamma^2/kR, \tag{2.21}$$

$$Q_1 = \theta_1 \frac{B}{R}\frac{(b-a)}{d} \quad \text{and} \quad Q_u = \theta_u \frac{B}{R}\frac{(b-a)}{d}. \tag{2.22}$$

Q_1 and Q_u are the ratio of the lower and upper boundary slopes to the slope of the isotherms.

When $F = Q_1 = Q_u = 0$ we have the Eady problem for which

$$\hat{c}^2 + [1 + \tfrac{1}{4}\gamma^2 - \gamma \coth\gamma]/\gamma^2 = 0, \tag{2.23}$$

where $\hat{c}$ is either real or pure imaginary according as

$$\gamma \gtrless 2.399. \tag{2.24}$$

The more complex behaviour of equation (2.19) when $F \neq 0$, $Q_1 \neq 0$ and $Q_u \neq 0$ is discussed in the following sections.

(*b*) *The energetics*

Consideration of the essential energetics of baroclinic instability (see Eady 1949) gives insight into some of the properties of equation (2.19). In the Eady problem (i.e. $Q_1 = Q_u = F = 0$) at 'low' rotation rates (i.e. $\gamma \geqslant 2.399$) the mean angle of fluid parcel interchange in the supposed sinusoidal disturbance occurs at angles higher than the isotherms (for a detailed discussion of the neutral waves see Bretherton 1966*a*). This leads to a neutral oscillatory solution. At more rapid rotation rates ($\gamma \geqslant 2.399$) the vertical stiffness of the fluid increases and the presence of the boundaries is felt throughout the interior of the fluid (cf. the Taylor–Proudman theorem (Greenspan 1968)). The fluid parcels are thus constrained to move on surfaces less inclined to the horizontal than the isotherms and release potential energy (see figure 6, cases (*a*), (*b*) and (*c*)) at a rate which increases at first as γ decreases, attains a maximum value and then decreases to zero when γ is so small that parcels are constrained to move almost horizontally (figure 6, case (*c*)). Thus maximum rate of energy release occurs when the parcels are interchanged at an angle roughly half way between the isotherms and the horizontal geopotentials (figure 6, case (*b*)).

If the boundaries are allowed to slope, but remain parallel, then the parcels will, as before, tend to move parallel to the boundaries, so that the energy release (which still depends on the angle of parcel interchange relative to the isotherms and the horizontal geopotentials) is affected by the change in boundary slope. In the laboratory experiments when the boundaries are sloped, other parameters such as the slope of the isotherms may change, but here in the context of the linear theory we assume that these other parameters are held fixed.

PHILOSOPHICAL TRANSACTIONS OF THE ROYAL SOCIETY A MATHEMATICAL, PHYSICAL & ENGINEERING SCIENCES

If the parallel boundaries slope at an angle less in magnitude, but in the same sense as the isotherms, i.e. $0 < Q_l = Q_u < 1$, the tendency for the parcels to move at angles shallower than the isotherms will be diminished and the marginally stable case in the Eady problem ($\gamma = 2.399$) will be stabilized (figure 6, case (d)). On the other hand at the highest rotation rates (figure 6, case (f)), rather than moving almost horizontally and releasing little energy, the parcels, in moving almost parallel to the boundaries will release more energy than they could if the boundaries were horizontal. If the boundary slope is equal to, or greater than, the slope of the isotherms, i.e. $Q_l = Q_u \geqslant 1$, the flow is always stable as no matter how rapid the rotation the parcels cannot move more horizontally than the boundaries and hence in this case more horizontally than the isotherms.

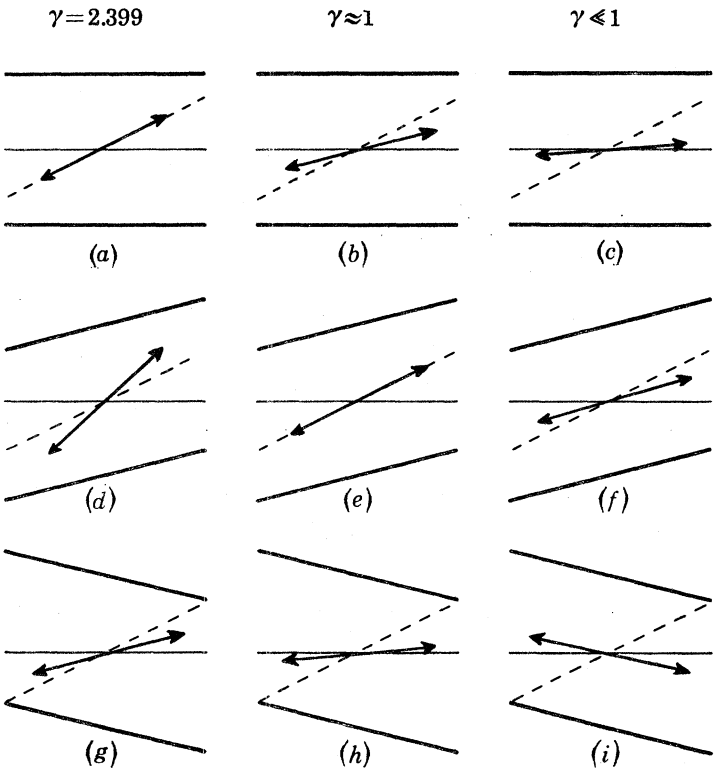

FIGURE 6. Illustrating the energetics of baroclinic instability with parallel sloping upper and lower boundaries (see text). ——, Upper and lower boundaries; ——, geopotential; – – –, isotherm; ←→, angle of parcel interchange.

If the parallel boundaries slope in the opposite sense to the isotherms, i.e. $Q_l = Q_u < 0$ then the marginally stable case of the Eady problem ($\gamma = 2.399$) will be destabilized (figure 6, case (g)). The high rotation rate case, where the angle of parcel interchange is almost parallel to the boundaries, will however be stabilized as the parcels will be interchanged at angles less than the horizontal (figure 6, case (i)).

It is clear from equation (2.19) that the effect of rotation in this problem depends specifically on the parameter γ (see equation (2.20)). Thus long waves are more strongly controlled by rotation than short waves and the marginally stable case of the Eady problem, which has been regarded above as occurring when the rotation is too low to constrain the angle of parcel interchange, may also be regarded as occurring when the wavelength is too short, and is termed

a 'short wave cut-off'. The stabilization at rapid rotation rates in the $Q_l = Q_u < 0$ case may correspondingly be termed a 'long wave cut-off'.

(c) *Special cases*

The calculations which follow are intended both to clarify the properties of equation (2.19) and to indicate possible effects in the parameter range of the experiments. To satisfy the latter requirement the calculations are given in terms of the dimensional variables of the experiments, i.e. in terms of varying Ω, $\Delta\rho$, Q_l and Q_u with other parameters fixed. The values of the parameters have been chosen to correspond to the mean values found in the experiments and the assumptions made in the theory are not fulfilled. In particular the values of Rossby number may be as large as 0.3 and thus not always $\ll 1$.

(i) *Parallel upper and lower boundaries*

Figure 7 shows contours of '*e*-folding' periods for an $m = 4$ mode on a graph of B against $|\theta_l|$, in which the variables are Ω, θ_l and θ_u, for $Q_l = Q_u \geqslant 0$, i.e. boundaries sloping in the same sense as the isotherms. The viscosity is zero and other parameters are as given in the legend. Where the contours intersect the $|\theta_l| = 0$ axis we have the Eady solution for which $Q_l = Q_u = F = 0$. For sufficiently high B the mode is stable but at $B = 0.302$ ($\gamma = 2.399$) the mode becomes unstable and as B decreases further the growth rates rise to a maximum and then fall to zero as B goes to zero ($\Omega \to \infty$). The effect of sloping the boundaries in this way is, as suggested in § 2 (*b*), to stabilize the mode by decreasing the value of B (i.e. increasing the value of Ω) at which the transition occurs, giving a complete stabilization of the mode when $Q_l = Q_u \geqslant 1$. However, the growth rate of any particular unstable mode is not always reduced and appreciable increases occur for small B and $Q_l = Q_u \approx \frac{1}{2}$.

Figure 8 is plotted in the same way as figure 7 but for the case of $Q_l = Q_u \leqslant 0$. In this case the 'Eady' transition is destabilized by increasing the value of B at which the mode becomes unstable. However, the maximum value of growth rate is decreased and the growth rates, rather than going to zero as B goes to zero, now go to zero at a small value of B (i.e. a long wave cut-off as predicted in § 2 (*b*)).

Figures 9 and 10 show, rather than growth rates for a single mode, modes of maximum growth rate for the cases $Q_u = Q_l > 0$ and $Q_u = Q_l < 0$ respectively. As before the variables are Ω, θ_l and θ_u but now $\nu = 0.01\ \mathrm{cm^2\,s^{-1}}$. The effect of the sloping boundaries on the various wave numbers is now evident: for a given value of B the wave number m of maximum growth rate is decreased for $Q_u = Q_l > 0$ and increased for $Q_u = Q_l < 0$. For $Q_u = Q_l > 0$ the effect of viscosity is slight, but for $Q_u = Q_l < 0$, this is not so owing to the reduced growth rates, and the instability is restricted to $|\theta_l| < 22°$.

(ii) *Oppositely sloping upper and lower boundaries*

For systems in which the upper and lower boundaries are parallel the unstable waves move with the mean flow, while the neutral waves propagate relative to it. In a barotropic fluid the variation of depth with radius produced by oppositely sloping boundaries is equivalent to a β-effect, giving rise to Rossby wave propagation relative to the mean flow (Veronis 1963). In a baroclinic fluid as we have here, the oppositely sloping boundaries are no longer completely equivalent to the β-effect (Bretherton 1966*b*; Green 1960), but propagation properties similar to those of Rossby waves occur. The stability properties, as we shall see below, are also affected but

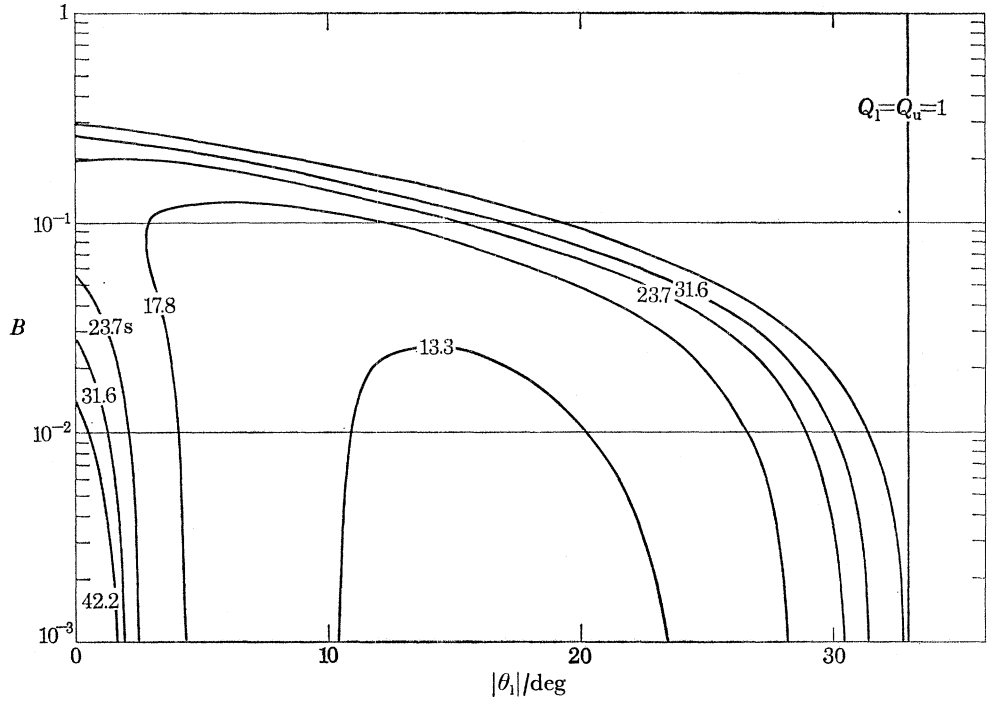

FIGURE 7. Growth rates for an $m = 4$ mode with $Q_l = Q_u > 0$, based on the extension of Eady's (1949) baroclinic instability theory to include sloping upper and lower boundaries (Hide 1969). The marginal stability envelope and contours of 'e-folding' times are given on a B against $|\theta_l|$ plot. The variables are Ω, Q_l and Q_u. The fixed parameters are $a = 3.80\,\text{cm}$, $b = 8.43\,\text{cm}$, $d = 12\,\text{cm}$, $\bar{\rho} = 1\,\text{g cm}^{-3}$, $\bar{\nu} = 0$, $\partial\rho/\partial z = -1.33 \times 10^{-4}\,\text{g cm}^{-4}$, $\partial\rho/\partial r = -0.86 \times 10^{-4}\,\text{g cm}^{-4}$.

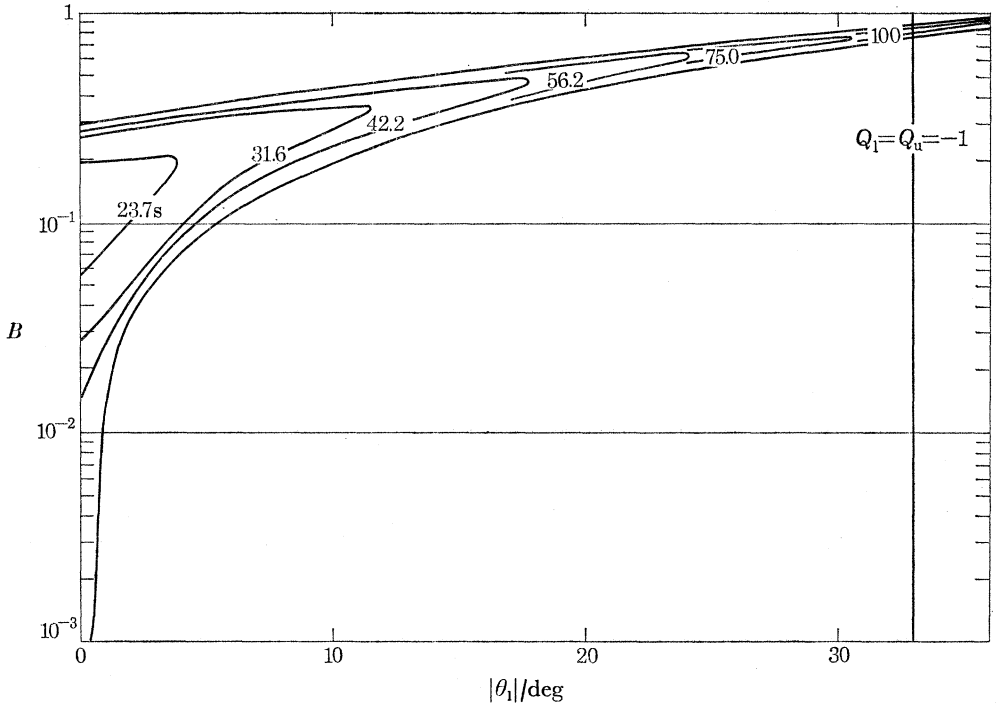

FIGURE 8. Growth rates for an $m = 4$ mode with $Q_l = Q_u < 0$, based on the extension of Eady's (1949) baroclinic instability theory to include sloping upper and lower boundaries (Hide 1969). The marginal stability envelope and contours of 'e-folding' times are given on a B against $|\theta_l|$ plot. The variables are Ω, Q_l and Q_u. The fixed parameters are $a = 3.80\,\text{cm}$, $b = 8.43\,\text{cm}$, $d = 12\,\text{cm}$, $\bar{\rho} = 1\,\text{g cm}^{-3}$, $\bar{\nu} = 0$, $\partial\rho/\partial z = -1.33 \times 10^{-4}\,\text{g cm}^{-4}$, $\partial\rho/\partial r = -0.86 \times 10^{-4}\,\text{g cm}^{-4}$.

PHILOSOPHICAL TRANSACTIONS OF THE ROYAL SOCIETY A MATHEMATICAL, PHYSICAL & ENGINEERING SCIENCES

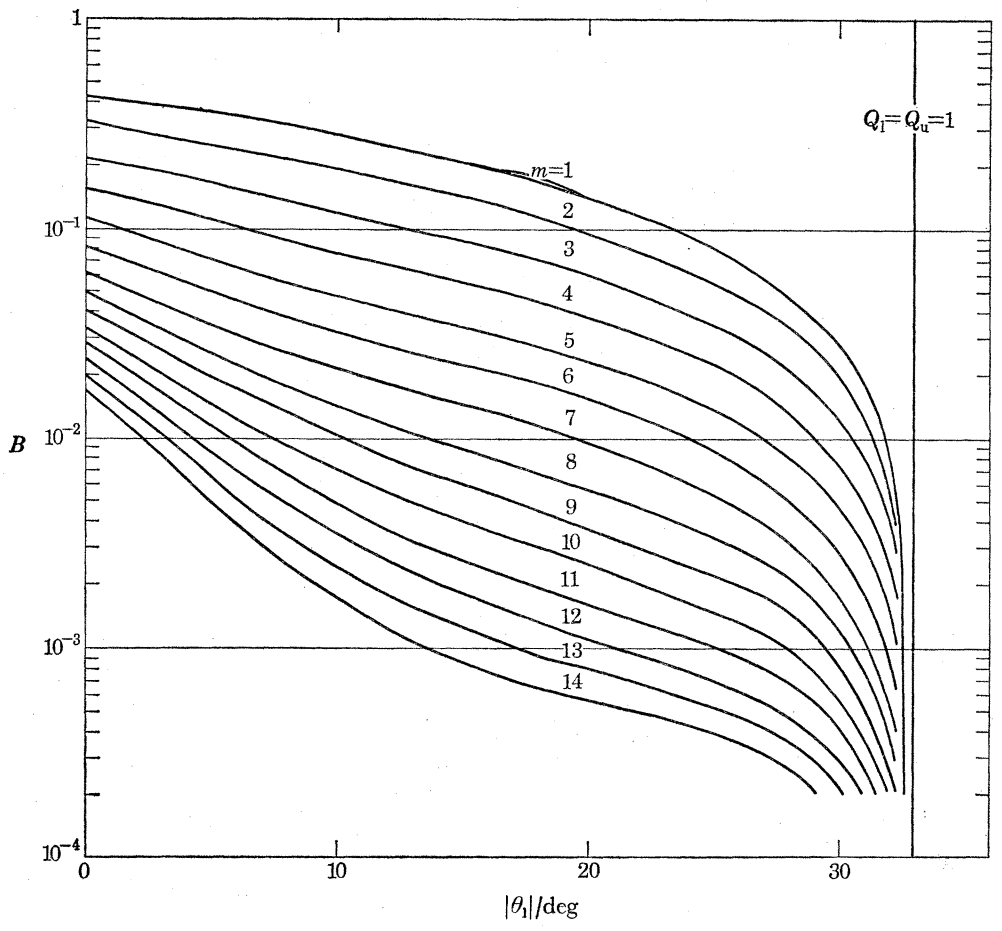

FIGURE 9. Modes ($m = 1$ to 14) of maximum instability with $Q_1 = Q_u > 0$, based on the extension of Eady's (1949) baroclinic instability theory to include sloping upper and lower boundaries (Hide 1969). The wave number of maximum instability transition curves are given on a B against $|\theta_1|$ plot. The variables are Ω, Q_1 and Q_u. The fixed parameters are $a = 3.80\,\text{cm}$, $b = 8.43\,\text{cm}$, $d = 12\,\text{cm}$, $\bar{\rho} = 1\,\text{g cm}^{-3}$, $\bar{\nu} = 0.01\,\text{cm}^2\,\text{s}^{-1}$, $\partial\rho/\partial z = -1.33 \times 10^{-4}\,\text{g cm}^{-4}$, $\partial\rho/\partial r = -0.86 \times 10^{-4}\,\text{g cm}^{-4}$.

the effects cannot be predicted by the 'energetic' arguments applied to the parallel boundary cases in §2(*b*).

Figure 11 shows contours of '*e*-folding' periods for an $m = 4$ mode on a graph of B against $|\theta_1|$, in which the variables are Ω, θ_u and θ_1, for $Q_1 = -Q_u$. The viscosity is zero and other conditions are as in the legend; this figure may be compared with figures 7 and 8 for parallel sloping boundaries. The effect of these boundaries is to stabilize the mode, the highest value of B at which waves occur is decreased and, as with the $Q_1 = Q_u < 0$ slopes, the mode is stable for small values of B. The mode is completely stabilized for $Q_1 = -Q_u \geqslant 1$. Figure 12 shows contours of non-dimensional drift rates for the mode of figure 11. Figure 13 shows modes of maximum growth rate for $\nu = 0.01\,\text{cm}^2\,\text{s}^{-1}$; the wave numbers of maximum growth rate are increased slightly.

(iii) *Horizontal upper boundaries and sloping lower boundaries*

Figure 14 shows growth rate contours for an $m = 4$ mode with $Q_1 > 0$, $Q_u = 0$, the viscosity is zero and other parameters are as before. A comparison with figures 7 and 11 shows the effects to be a combination of those seen with $Q_1 = Q_u > 0$ (figure 7) and $Q_1 = -Q_u$ (figure 11). Because

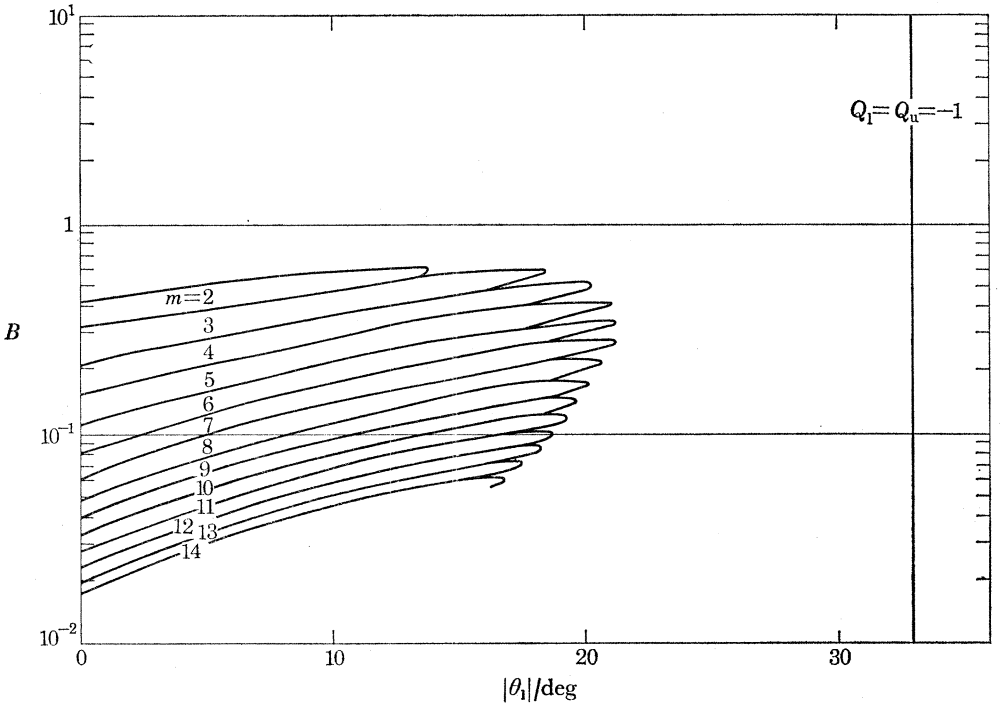

FIGURE 10. Modes ($m = 1$ to 14) of maximum instability with $Q_l = Q_u < 0$, based on the extension of Eady's (1949) baroclinic instability theory to include sloping upper and lower boundaries (Hide 1969). The wave number of maximum instability transition curves are given on a B against $|\theta_l|$ plot. The variables are Ω, Q_l and Q_u. The fixed parameters are $a = 3.80\,\text{cm}$, $b = 8.43\,\text{cm}$, $d = 12\,\text{cm}$, $\bar{\rho} = 1\,\text{g cm}^{-3}$, $\bar{\nu} = 0.01\,\text{cm}^2\,\text{s}^{-1}$, $\partial\rho/\partial z = -1.33 \times 10^{-4}\,\text{g cm}^{-4}$, $\partial\rho/\partial r = -0.86 \times 10^{-4}\,\text{g cm}^{-4}$.

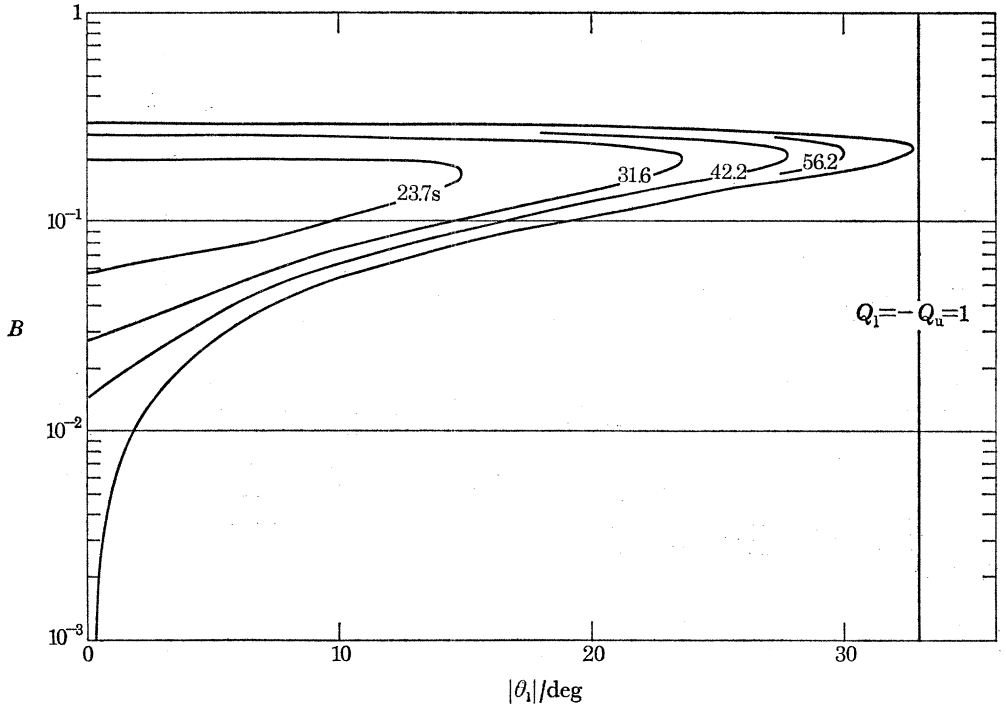

FIGURE 11. Growth rates for an $m = 4$ mode with $Q_l = -Q_u$, based on the extension of Eady's (1949) baroclinic instability theory to include sloping upper and lower boundaries (Hide 1969). The marginal stability envelope and contours of 'e-folding' times are given on a B against $|\theta_l|$ plot. The variables are Ω, Q_l and Q_u. The fixed parameters are $a = 3.80\,\text{cm}$, $b = 8.43\,\text{cm}$, $d = 12\,\text{cm}$, $\bar{\rho} = 1\,\text{g cm}^{-3}$, $\bar{\nu} = 0$, $\partial\rho/\partial z = -1.33 \times 10^{-4}\,\text{g cm}^{-4}$, $\partial\rho/\partial r = -0.86 \times 10^{-4}\,\text{g cm}^{-4}$.

PHILOSOPHICAL TRANSACTIONS OF THE ROYAL SOCIETY A MATHEMATICAL, PHYSICAL & ENGINEERING SCIENCES

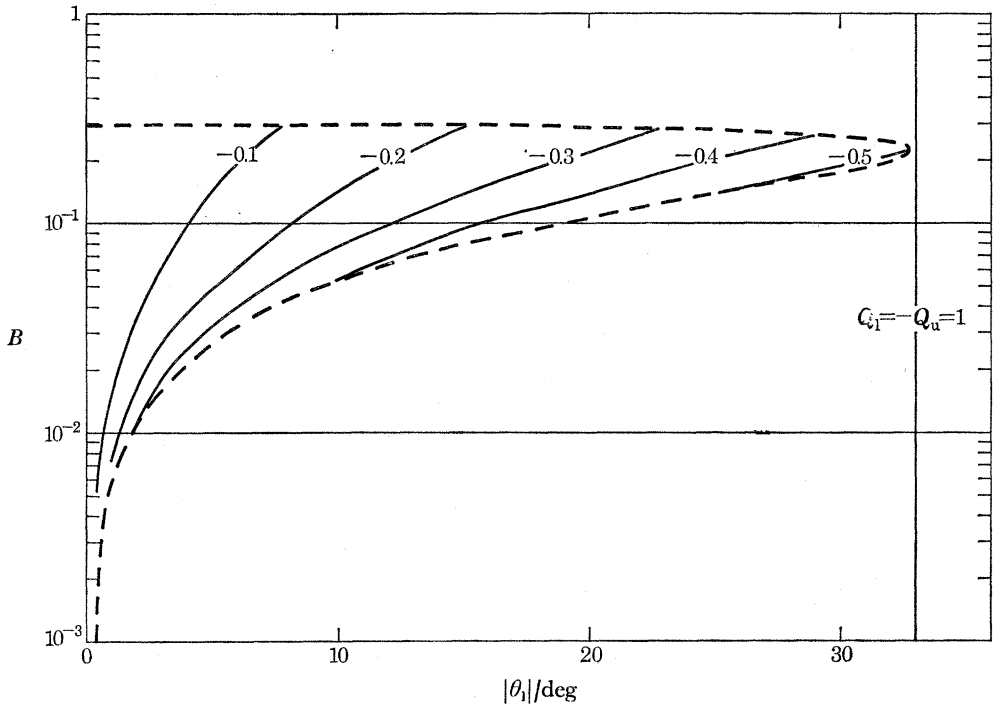

FIGURE 12. Drift rates for an $m = 4$ mode with $Q_l > 0$ and $Q_l = Q_u$ based on the extension of Eady's (1949) baroclinic instability theory to include sloping upper and lower boundaries (Hide 1969). The marginal stability envelope and contours of non-dimensional drift velocities are given on a B against $|\theta_l|$ plot. The variables are Ω, Q_l and Q_u. The fixed parameters are: $a = 3.80$ cm, $b = 8.43$ cm, $d = 12$ cm, $\bar{\rho} = 1\,\mathrm{g\,cm^{-3}}$, $\bar{\nu} = 0$, $\partial\rho/\partial z = -1.33 \times 10^{-4}\,\mathrm{g\,cm^{-4}}$, $\partial\rho/\partial r = -0.86 \times 10^{-4}\,\mathrm{g\,cm^{-4}}$.

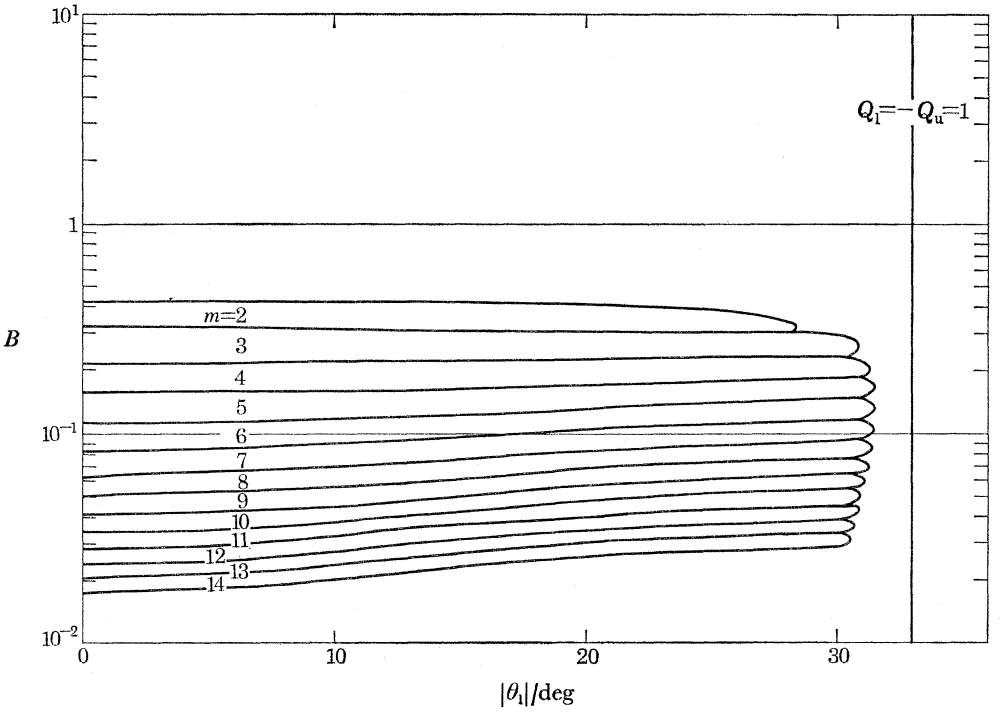

FIGURE 13. Modes ($m = 1$ to 14) of maximum instability with $Q_l = -Q_u$, based on the extension of Eady's (1949) baroclinic instability theory to include sloping upper and lower boundaries (Hide 1969). The wave number of maximum instability transition curves are given on a B against $|\theta_l|$ plot. The variables are Ω, Q_l and Q_u. The fixed parameters are $a = 3.80$ cm, $b = 8.43$ cm, $d = 12$ cm, $\bar{\rho} = 1\,\mathrm{g\,cm^{-3}}$, $\bar{\nu} = 0.01\,\mathrm{cm^2\,s^{-1}}$, $\partial\rho/\partial z = -1.33 \times 10^{-4}\,\mathrm{g\,cm^{-4}}$, $\partial\rho/\partial r = -0.86 \times 10^{-4}\,\mathrm{g\,cm^{-4}}$.

PHILOSOPHICAL TRANSACTIONS OF THE ROYAL SOCIETY A MATHEMATICAL, PHYSICAL & ENGINEERING SCIENCES

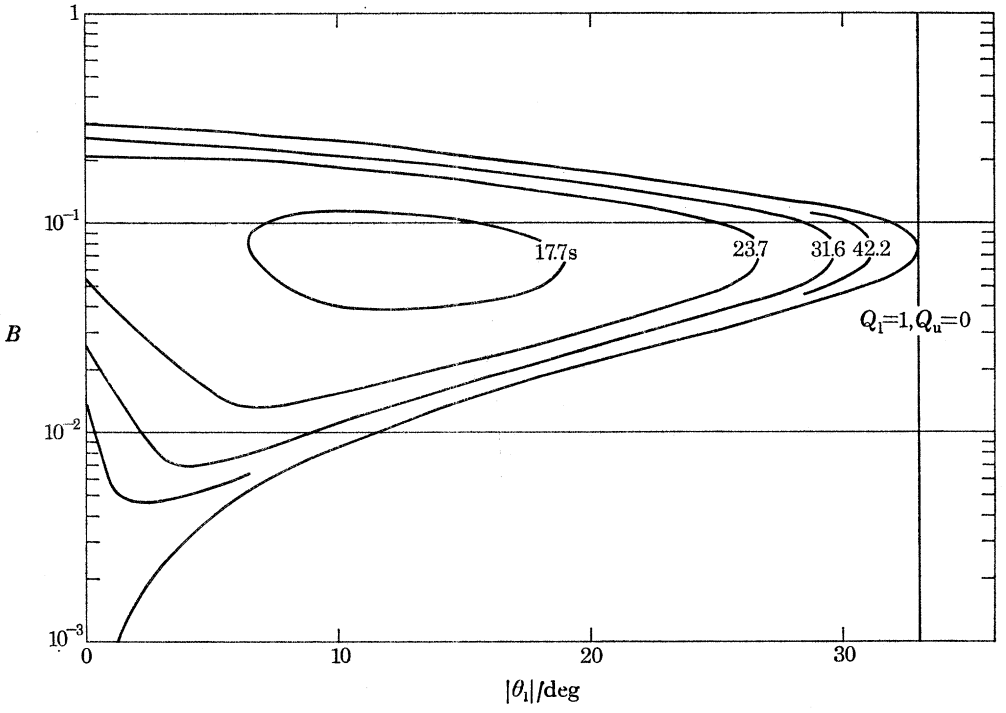

FIGURE 14. Growth rates for an $m = 4$ mode with $Q_l > 0$, $Q_u = 0$, based on the extension of Eady's (1949) baroclinic instability theory to include sloping upper and lower boundaries (Hide 1969). The marginal stability envelope and contours of 'e-folding' times are given on a B against $|\theta_l|$ plot. The variables are Ω, Q_l and Q_u. The fixed parameters are $a = 3.80\,\text{cm}$, $b = 8.43\,\text{cm}$, $d = 12\,\text{cm}$, $\bar{\rho} = 1\,\text{g cm}^{-3}$, $\bar{\nu} = 0$, $\partial\rho/\partial z = -1.33 \times 10^{-4}\,\text{g cm}^{-4}$, $\partial\rho/\partial r = -0.86 \times 10^{-4}\,\text{g cm}^{-4}$.

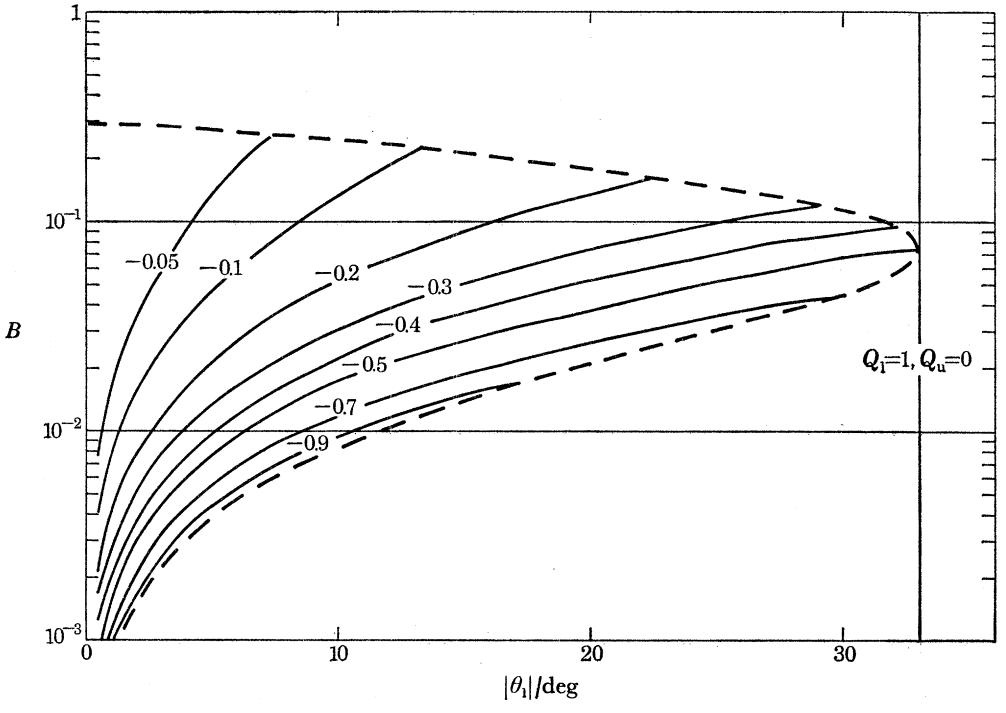

FIGURE 15. Drift rates for an $m = 4$ mode with $Q_l > 0$ and $Q_u = 0$ based on the extension of Eady's (1949) baroclinic instability theory to include sloping upper and lower boundaries (Hide 1969). The marginal stability envelope and contours of non-dimensional drift velocities are given on a B against $|\theta_l|$ plot. The variables are Ω, Q_l and Q_u. The fixed parameters are: $a = 3.80\,\text{cm}$, $b = 8.43\,\text{cm}$, $d = 12\,\text{cm}$, $\bar{\rho} = 1\,\text{g cm}^{-3}$, $\bar{\nu} = 0$, $\partial\rho/\partial z = -1.33\,\text{g cm}^{-4}$, $\partial\rho/\partial r = -0.86 \times 10^{-4}\,\text{g cm}^{-4}$.

PHILOSOPHICAL TRANSACTIONS OF THE ROYAL SOCIETY A MATHEMATICAL, PHYSICAL & ENGINEERING SCIENCES

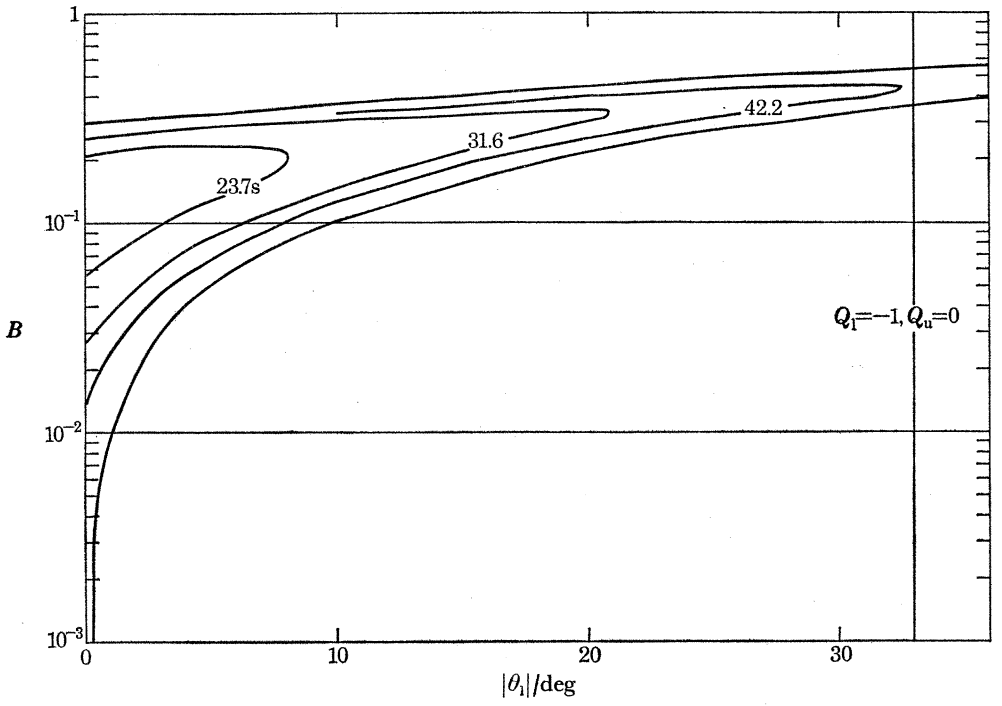

FIGURE 16. Growth rates for an $m = 4$ mode with $Q_l < 0$, $Q_u = 0$, based on the extension of Eady's (1949) baroclinic instability theory to include sloping upper and lower boundaries (Hide 1969). The marginal stability envelope and contours of 'e-folding' times are given on a B against $|\theta_l|$ plot. The variables are Ω, Q_l and Q_u. The fixed parameters are $a = 3.80\,\text{cm}$, $b = 8.43\,\text{cm}$, $d = 12\,\text{cm}$, $\bar{\rho} = 1\,\text{g cm}^{-3}$, $\bar{\nu} = 0$, $\partial\rho/\partial z = -1.33 \times 10^{-4}\,\text{g cm}^{-4}$, $\partial\rho/\partial r = -0.86 \times 10^{-4}\,\text{g cm}^{-4}$.

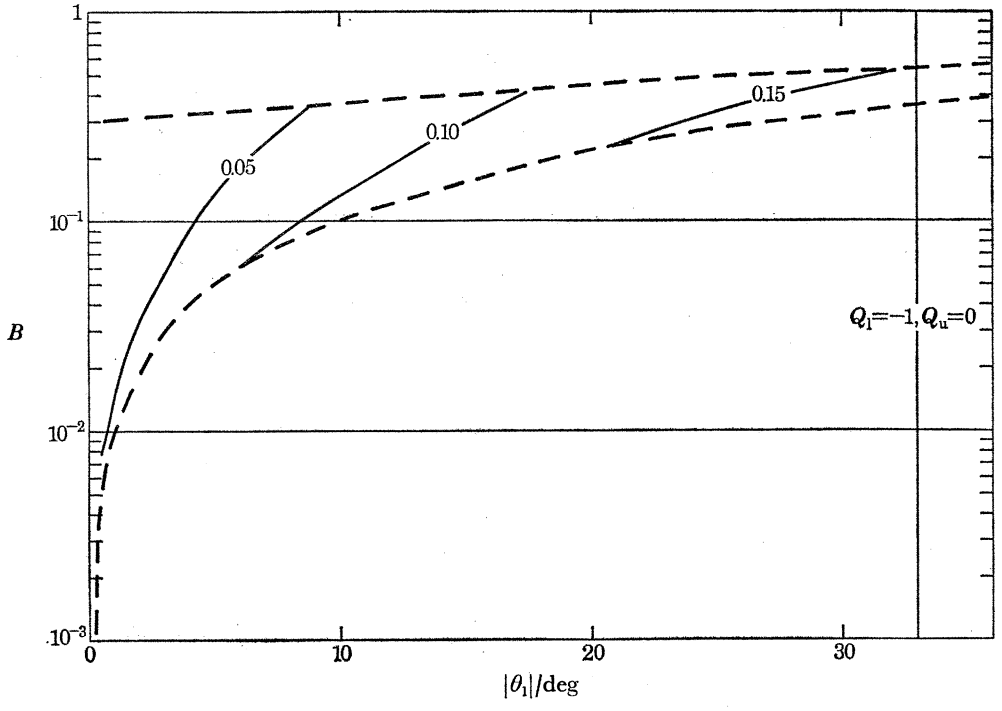

FIGURE 17. Drift rates for an $m = 4$ mode with $Q_l < 0$ and $Q_u = 0$ based on the extension of Eady's (1949) baroclinic instability theory to include sloping upper and lower boundaries (Hide 1969). The marginal stability envelope and contours of non-dimensional drift velocities are given on a B against $|\theta_l|$ plot. The variables are Ω, Q_l and Q_u. The fixed parameters are: $a = 3.80\,\text{cm}$, $b = 8.43\,\text{cm}$, $d = 12\,\text{cm}$, $\bar{\rho} = 1\,\text{g cm}^{-3}$, $\bar{\nu} = 0$, $\partial\rho/\partial z = -1.33 \times 10^{-4}\,\text{g cm}^{-4}$, $\partial\rho/\partial r = -0.86 \times 10^{-4}\,\text{g cm}^{-4}$.

PHILOSOPHICAL TRANSACTIONS OF THE ROYAL SOCIETY A MATHEMATICAL, PHYSICAL & ENGINEERING SCIENCES

of the variation of depth with radius the waves drift relative to the mean flow and figure 15 shows the non-dimensional drift speeds. In non-dimensional units the magnitude of maximum and minimum flow velocities of the basic state is 0.5. Figure 16 shows growth rate contours for an $m = 4$ mode with $Q_l < 0$, $Q_u = 0$. The viscosity is zero and other parameters as before. A comparison with figures 8 and 11 shows the effect to be similar to those seen with $Q_l = Q_u < 0$. The phase speeds for this mode are given in figure 17.

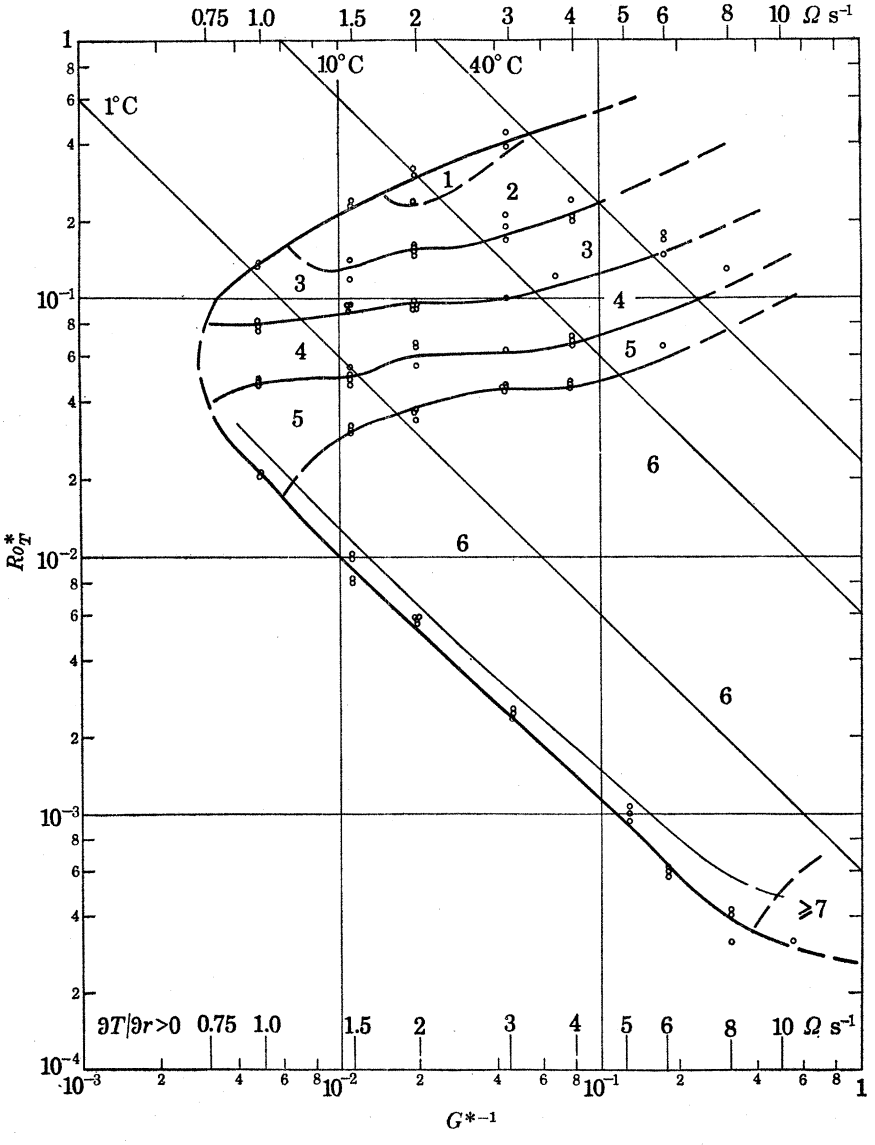

FIGURE 18. Régime diagram for $T_a < T_b$ (after Fultz 1964). $Ro_T^* = gd\alpha\,\partial T/\partial r/2\Omega^2 b$ and $G^{*-1} = \Omega^2 b/g$ where $\partial T/\partial r$ is based on internal temperature measurements. Experimental details: working fluid water with upper surface free; $a = 2.45$ cm, $b = 6.02$ cm, $d = 13.0$ cm. $\bar{\nu} = 1.0 \times 10^{-2}$ cm^2 s^{-1}, $\bar{\rho} = 0.998$ g cm^{-3}.

(*d*) *Régime diagrams*

(i) *Previous experiments*

Systematic variations of the experimental parameters (Fowlis & Hide 1965) have led to the presentation of results on régime diagrams with $\Theta = gd|\Delta\rho|/\bar{\rho}\Omega^2(b-a)^2$ ($|\Delta\rho|/\bar{\rho} = \alpha|\Delta T|$, where

$\Delta T = T_b - T_a$) as ordinate and $\mathscr{T} = 4\Omega^2(b-a)^5/\bar{\nu}^2 d$ as abscissa. In these diagrams non-axisymmetric flow occurs inside an anvil-shaped region. Figure 3 shows the measurements of Fowlis & Hide (1965) which are for an annulus with a free upper surface and the inner wall cooled; the positions of the upper symmetric, lower symmetric, regular and irregular régimes are indicated.

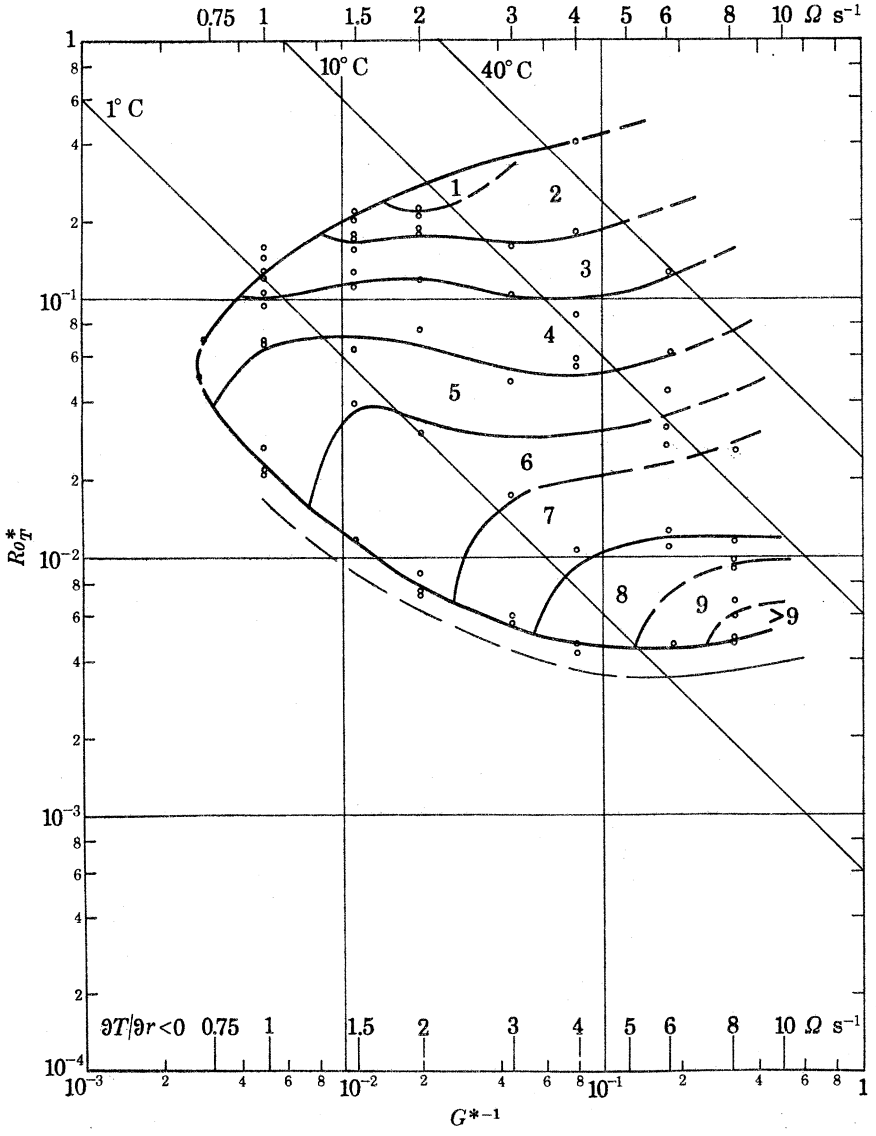

FIGURE 19. Régime diagram for $T_a > T_b$ (after Fultz 1964). $Ro_T^* = gd\alpha\,\partial T/\partial r/2\Omega^2 b$ and $G^{*-1} = \Omega^2 b/g$ where $\partial T/\partial r$ is based on internal temperature measurements. Experimental details: working fluid water with upper surface free; $a = 2.45$ cm, $b = 6.02$ cm, $d = 13.0$ cm, $\bar{\nu} = 1.01 \times 10^{-2}$ cm^2 s^{-1}, $\bar{\rho} = 0.998$ g cm^{-3}.

Owing to the fairly uniform variation of the internal temperature structure with rotation rate and the magnitude of ΔT, similar diagrams are obtained with abscissa based on the external, the internal horizontal, or the internal vertical temperature difference. Figures 18 and 19 show the measurements of Fultz (1964) for an annulus with the inner and outer walls cooled respectively.

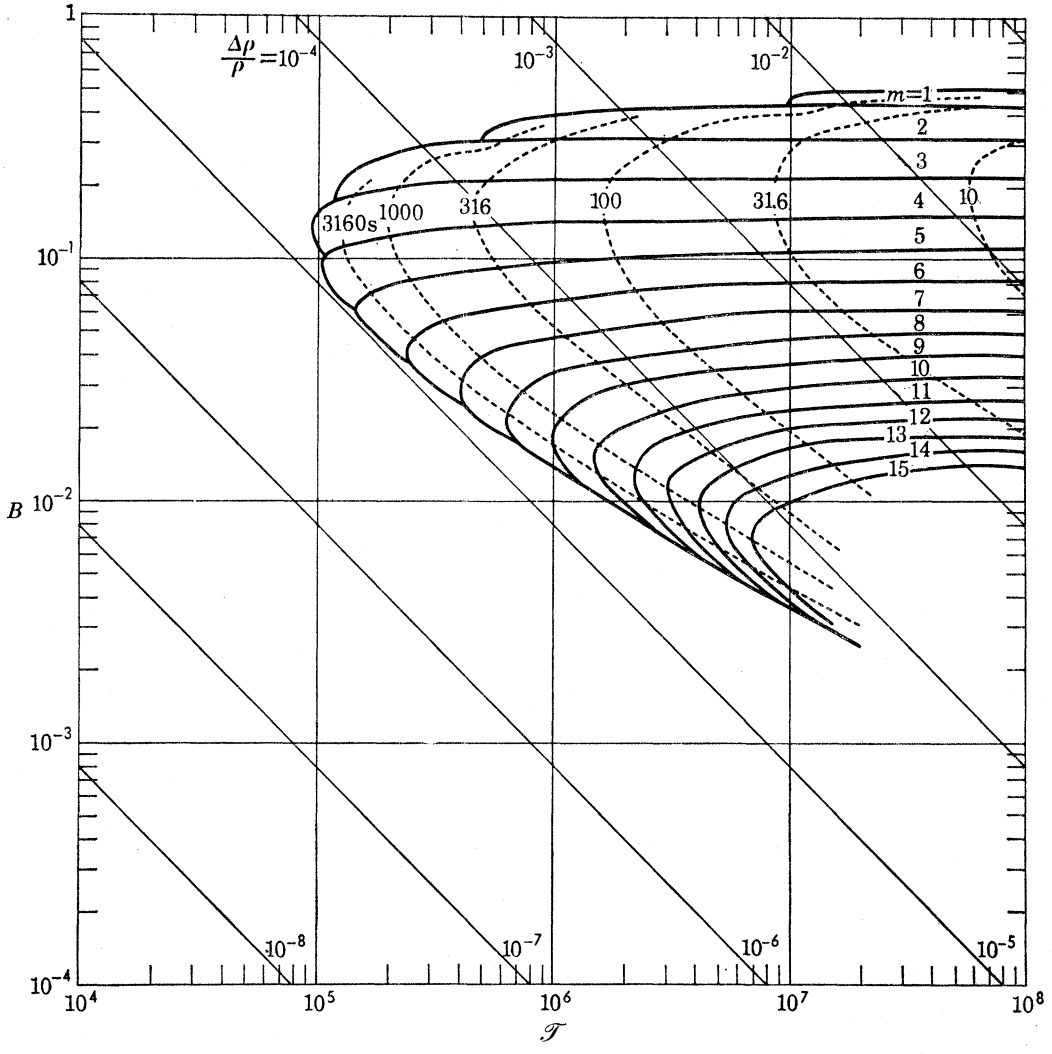

FIGURE 20. Régime diagram for $Q_1 = Q_u = 0$ based on the extension of Eady's (1949) baroclinic instability theory to include Ekman layers (Barcilon 1964; Hide 1969). The wave number of maximum instability transition curves and contours of the 'e-folding' times are given on a B against $\mathscr{T}$ plot. The variables are Ω and $\Delta\rho$. The fluid parameters are: $a = 3.80\,\mathrm{cm}$, $b = 8.43\,\mathrm{cm}$, $d = 12\,\mathrm{cm}$, $\bar{\rho} = 1\,\mathrm{g\,cm^{-3}}$, $\bar{\nu} = 0.01\,\mathrm{cm^2\,s^{-1}}$ and $(\partial\rho/\partial z)/(\partial\rho/\partial r) = 1.55$ where $\Delta\rho = d\,|\partial\rho/\partial z| + (b-a)\,|\partial\rho/\partial r|$.

(ii) *Comparison between previous experiments and linear theory for flat geopotentials* ($\theta_1 = \theta_u = 0$)

A number of previous workers (see, for example, Fowlis & Hide 1965; Kaiser 1970) have compared the experimental régime diagrams (figures 3, 18 and 19) with the results of linear theory. There is, however, an important difficulty in the comparison: in the experiments the slope of the isotherms not only varies through the fluid (while constant in the linear theory) but also with the parameters B and $\mathscr{T}$. The variations through the fluid must be ignored in a comparison with the linear theory but allowance should be made for the variation of the mean isotherm slope with B and $\mathscr{T}$. In practice there is insufficient experimental data on the slope of the isotherms for this to be done and instead a single value (33° used in the present calculations) typical of the experiments is taken. Figure 20 is calculated in this way, and for parameters similar to those in figures 3, 18 and 19, it shows modes of maximum instability and their growth rates. The boundaries are assumed horizontal ($\theta_1 = \theta_u = 0$) and, except that the aspect ratio has not been

taken as unity, this corresponds to the situation treated by Barcilon (1964). The best agreement between the experiments and linear theory is obtained in the inviscid limit at high $\mathscr{T}$ for the value of B at the transition from the wave régime to the upper symmetric régime (upper symmetric transition). The value of $\mathscr{T}$ at the 'knee' of the régime diagram seems on the face of it to be in reasonable agreement with the experiments (see Kaiser 1970), but if a value of isotherm slope appropriate to the knee were used in the calculation (about 60°) it would be evident that there is much more friction in the experimental system than the theoretical one. This extra dissipation can only be accounted for by side wall and internal friction (Fowlis & Hide 1965; Douglas & Mason 1973). The transition from the wave régime to the lower symmetric régime (lower symmetric transition) is in poor agreement with the theory. The experiments show marked changes with the sign of $\partial T/\partial r$ whereas in the theory with $\theta_l = \theta_u = 0$ the results are independent of the sign of $\partial T/\partial r$.

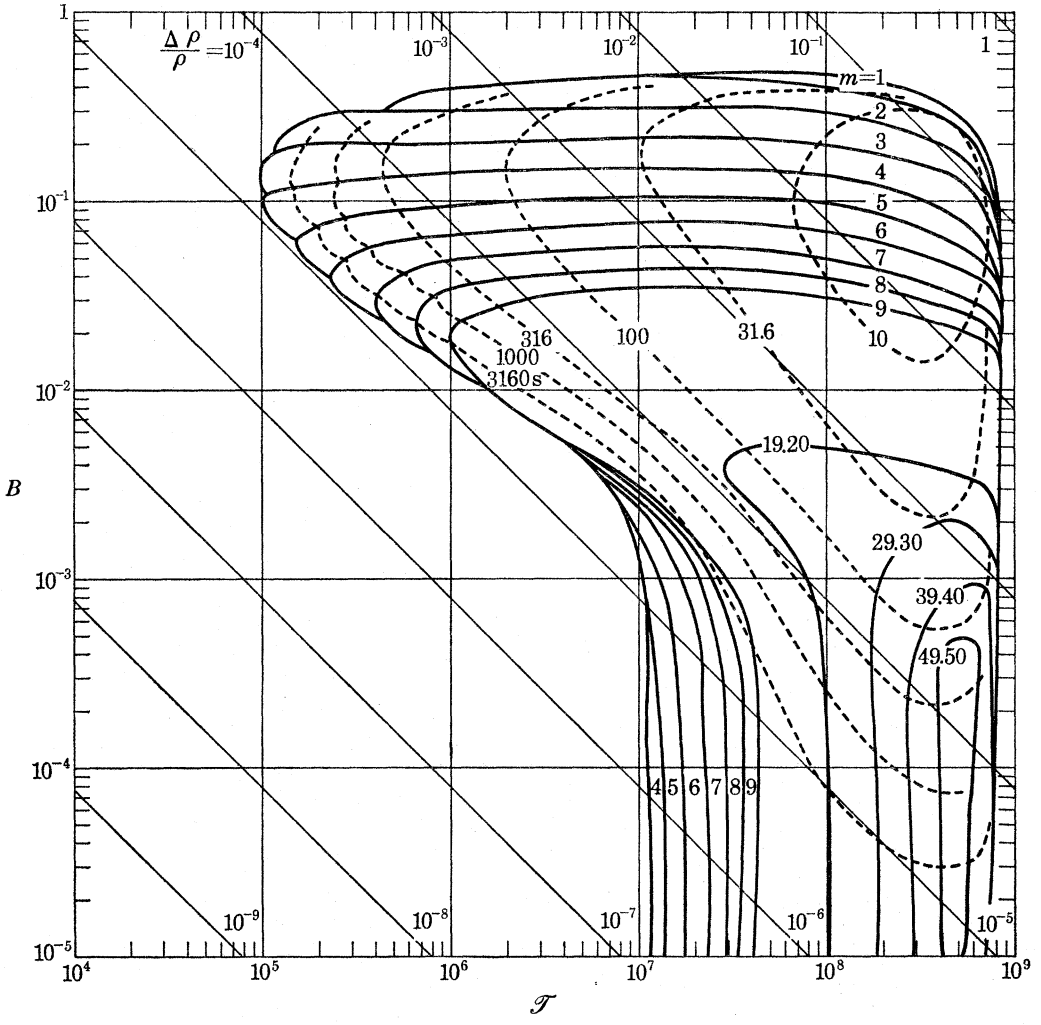

FIGURE 21. Régime diagram for the lower boundary sloping in the opposite sense but same magnitude as the geopotentials at $r = \frac{1}{2}(a+b)$ with $\partial T/\partial r > 0$, i.e. $Q_l > 0$ and $Q_u = 0$. This calculation is based on the extension of Eady's (1949) baroclinic instability theory to include the effects of both Ekman layers and sloping upper and lower boundaries (Hide 1969). The wavenumber of maximum instability transition curves and contours of 'e-folding' times of the most unstable waves are given on a B against $\mathscr{T}$ plot. The variables are Ω and $\Delta\rho$. The fixed parameters are: $a = 3.80$ cm, $b = 8.43$ cm, $d = 12$ cm, $\bar{\rho} = 1$ g cm^{-3}, $\bar{\nu} = 0.01$ cm^2 s^{-1} and $(\partial\rho/\partial z)/(\partial\rho/\partial r) = 1.55$ where $\Delta\rho = d\,|\partial\rho/\partial z| + (b-a)\,|\partial\rho/\partial r|$.

(iii) *Comparison between previous experiments and the predictions of a linear theory which models the effects of sloping geopotentials*

The dependence, in the experiments, of the lower symmetric transition on the sign of $\partial T/\partial r$ suggests an asymmetry not present in the $\theta_l = \theta_u = 0$ theory. One such asymmetry is due to the slope of geopotentials in a rotating frame. Within the context of the small angles of slope implied by the linear theory there is no difference between sloping the boundaries or the geopotentials and it is convenient to model the latter by sloping the boundaries. The calculations given here are for a rigid horizontal upper boundary with a rigid lower boundary sloping in the opposite sense but with the same magnitude as the geopotential slope at $r = \frac{1}{2}(a+b)$. Figures 21 and 22 show the modes of maximum instability and their growth rates on a $B:\mathscr{T}$ plot for $\partial T/\partial r > 0$ and $\partial T/\partial r < 0$ respectively. In the $\partial T/\partial r > 0$ case, the lower symmetric transition away from the knee

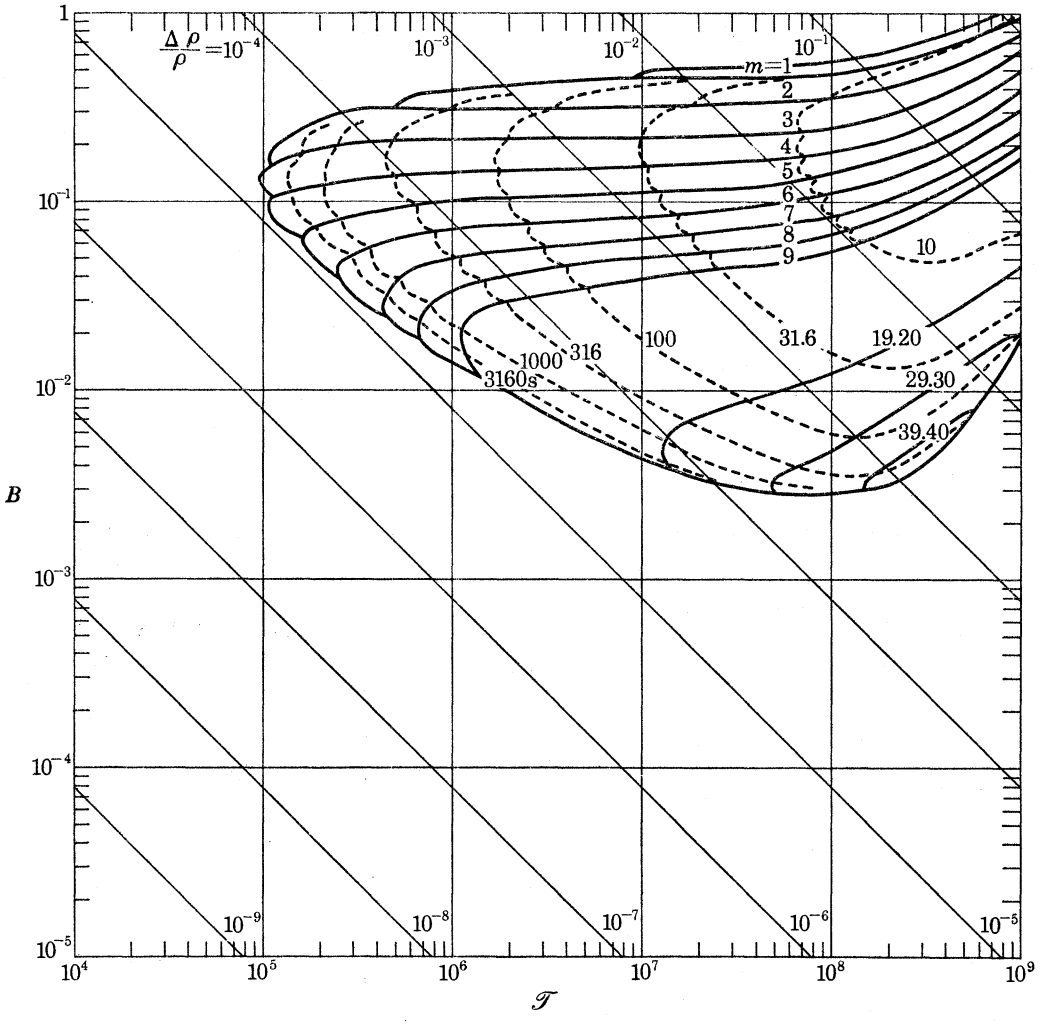

FIGURE 22. Régime diagram for the lower boundary sloping in the opposite sense but same magnitude as the geopotentials at $r = \frac{1}{2}(a+b)$ with $\partial T/\partial r < 0$, i.e. $Q_l < 0$ and $Q_u = 0$. This calculation is based on the extension of Eady's (1949) baroclinic instability theory to include the effects of both Ekman layers and sloping upper and lower boundaries (Hide 1969). The wavenumber of maximum instability transition curves and contours of '*e*-folding' times of the most unstable waves are given on a B against $\mathscr{T}$ plot. The variables are Ω and $\Delta\rho$. The fixed parameters are: $a = 3.80\,\text{cm}$, $b = 8.43\,\text{cm}$, $d = 12\,\text{cm}$, $\bar{\rho} = 1\,\text{g cm}^{-3}$, $\bar{\nu} = 0.01\,\text{cm}^2\,\text{s}^{-1}$ and $(\partial\rho/\partial z)/(\partial\rho/\partial r) = 1.55$ where $\Delta\rho = d|\partial\rho/\partial z| + (b-a)\,|\partial\rho/\partial r|$.

is destabilized whereas in the $\partial T/\partial r < 0$ case it is stabilized. Comparison with the experimental curves of figures 18 and 19 shows a striking qualitative similarity and the quantitative agreement between experiment and theory obtained below in § 4 (*b*) provides strong evidence that the shape of the lower symmetric transition is indeed due to the slope of the geopotentials.

3. Apparatus and experimental procedure

The ranges of experimental conditions covered by the investigation are summarized in table 1. The apparatus used was similar in its basic design to that used in previous experiments (Hide 1953, 1958; Fowlis & Hide 1965; Kaiser 1970), and in what follows attention has been restricted to the essential and novel features.

Table 1. Values of experimental parameters

parameter	value or approximate range
a/cm	3.80
b/cm	8.43
d/cm	12
Ω/rad s^{-1}	0–4
$\lvert T_b - T_a\rvert$/K	10†, 3‡
$\lvert\rho(T_b) - \rho(T_a)\rvert$/g cm^{-3}	2×10^{-3}†, 0.8×10^{-3}‡
$\bar{\nu}$/cm^2 s^{-1}	1.01×10^{-2}†, 1.5×10^{-2}‡
$\bar{\kappa}$/J cm^{-1} s^{-1} K^{-1}	5.86×10^{-3}†, 5.32×10^{-3}‡
$\bar{c}$/J g^{-1} K^{-1}	4.18†, 3.98‡
$\bar{\chi}$/cm^2 s^{-1}	1.41×10^{-3}†, 1.29×10^{-3}‡
$\bar{\rho}$/g cm^{-3}	0.998†, 1.037‡
θ_l/angular degrees	−36, −12, 0, 12, 36
θ_u/angular degrees	−36, −12, 0, 12, 36

† Liquid used: water. ‡ Liquid used: water–glycerol solution.

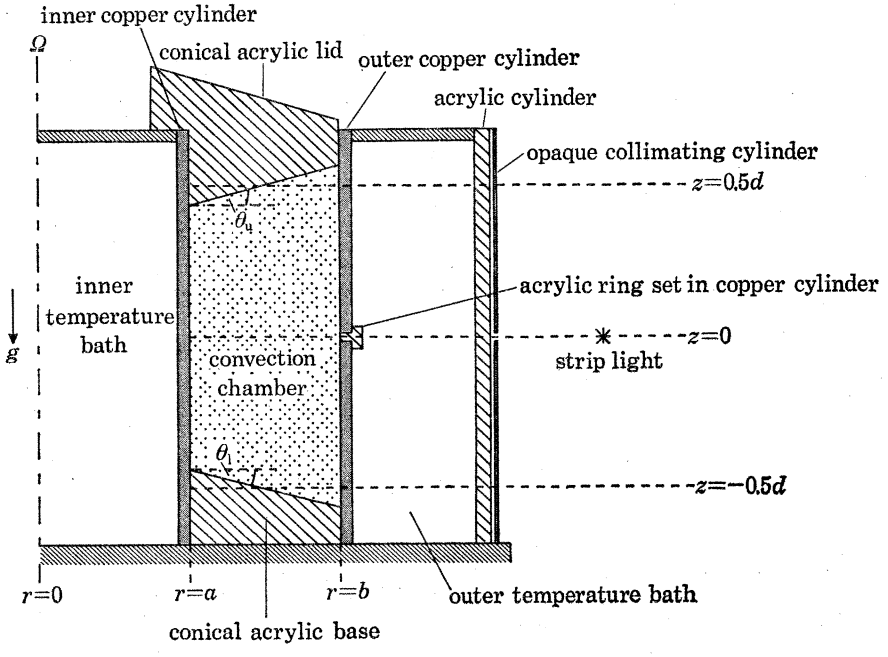

Figure 23. Schematic diagram of the apparatus showing the arrangement used to produce the sloping upper and lower boundaries. (r, ϕ, z) are cylindrical polar coordinates of a general frame moving with the apparatus, which rotates uniformly with angular velocity Ω about a vertical axis relative to the laboratory (inertial) frame.

(*a*) *Convection chamber*

The convection chamber (see figure 23) is the annular space of total height 18 cm between two concentric vertical cylinders, the inner one with outer radius $a = 3.80$ cm and the outer one with inner radius $b = 8.43$ cm. The cylinders were secured to a thermally insulating phenolic laminate baseplate mounted on a horizontal turntable. The inner cylinder was made entirely of copper. The outer cylinder consisted of two identical separate cylinders separated by a clear acrylic ring of thickness 0.5 cm (see figure 23). This acrylic ring was bonded to the copper by silicone rubber adhesive, and enabled a flat horizontal beam of light to enter the centre of the convection chamber whilst maintaining the advantages of a copper boundary wall to the convection chamber. A good thermally conducting bounding wall helps prevent the occurrence of large temperature gradients in the wall and enables the wall temperature to be specified accurately.

The effective bottom of the convection chamber was the upper surface of an annular acrylic base which projected above the floors of the inner and outer water baths. The acrylic base was interchangeable with other bases whose upper surfaces were parts of circular cones of varying slopes ($-36°$, $-12°$, 0, $12°$, $36°$). The height of these slopes at $r = \frac{1}{2}(a+b)$ was taken as $-\frac{1}{2}d$. The top of the convection chamber carried a clear acrylic lid. In experiments with a rigid upper surface the bottom of this lid was in contact with the fluid in the convection chamber. The lid was interchangeable with other lids whose bottom surfaces were parts of circular cones of varying slopes ($-36°$, $-12°$, 0, $12°$, $36°$). The height of these slopes at $r = \frac{1}{2}(a+b)$ was taken as $\frac{1}{2}d$. Thus, by means of these interchangeable bases and lids, a variety of configurations of sloping upper and lower surfaces was easily obtainable. In other experiments with a free liquid surface, a different lid was used which did not touch the liquid in the convection chamber but served to eliminate wind stress and reduce evaporation.

The gap width deviated from its mean value of 4.63 cm by less than 10^{-3} cm (as a result of very slight but unavoidable eccentricities of the cylinders) and the axis of the rotating apparatus deviated from the vertical by less than 10^{-4} rad. The errors in the vertical alinement of the cylinders and in the slope of the various bases and lids was less than 10^{-3} rad. The depth of the fluid at $r = \frac{1}{2}(a+b)$ was nominally 12 cm and the bases and lids were designed so that the middle of the clear acrylic ring in the outer cylinder was at $z = 0$. With a rigid lid in contact with the upper surface the depth of the fluid was measured with a rule to an accuracy of ± 0.2 mm, but with a free liquid surface a dipstick method was employed and the error was ± 0.5 mm.

(*b*) *Turntable*

The turntable was driven by a synchronous induction motor *via* a Graham continuously-variable speed transmission unit. Typical values of Ω were 0–4 rad s^{-1} and were maintained constant to an accuracy of 0.1 % over periods of the order of 0.5 h and to 0.5 % over several hours. Individual rotation periods could be measured by means of an electronic timing-unit actuated when a beam of light from a lamp fixed in the laboratory was reflected by a plane mirror mounted on the turntable on to a photo-cell fixed in the laboratory.

(*c*) *Temperature control and measurement*

The temperature baths in contact with the copper side walls (see figure 4.1) were supplied individually with water circulating at about 60 $cm^3 s^{-1}$ and kept at constant temperature to within ± 0.01 K by means of thermostats and smoothing baths. The temperatures of the inner

PHILOSOPHICAL TRANSACTIONS OF THE ROYAL SOCIETY A MATHEMATICAL, PHYSICAL & ENGINEERING SCIENCES

and outer walls, T_a and T_b, were taken as the average readings of four copper–constantan thermocouples mounted at different levels on both the inner and outer cylinders. The thermocouple junctions were glued with epoxy resin into narrow grooves on the outside of the outer copper cylinder and the inside of the inner copper cylinder. In spite of the rapid water circulation in the temperature baths and the high thermal conductivity of the copper cylinders, vertical temperature differences of about 5 % of $(T_b - T_a)$ were present in the cylinders. Thus the maximum temperature difference applied to the fluid is in fact about 5 % greater than $(T_b - T_a)$ measured in these experiments.

The temperatures in the interior of the convecting fluid were measured by thermocouples in one of two arrays. The positions (r, ϕ, z) of the thermocouples in these arrays were:

I. $[\frac{1}{2}(a+b), 0, -\frac{5}{12}d]; [\frac{1}{2}(a+b), 0, 0]; [\frac{1}{2}(a+b), 0, \frac{5}{12}],$

II. $[\frac{1}{4}(3a+b), 0, -\frac{3}{8}d]; [\frac{1}{2}(a+b), 0, -\frac{3}{8}d]; [\frac{1}{4}(a+3b), 0, -\frac{3}{8}d],$
$[\frac{1}{4}(3a+b), 0, 0]; [\frac{1}{2}(a+b), 0, 0]; [\frac{1}{4}(a+3b), 0, 0],$
$[\frac{1}{4}(3a+b), 0, \frac{3}{8}d]; [\frac{1}{2}(a+b), 0, \frac{3}{8}d]; [\frac{1}{4}(a+3b), 0, \frac{3}{8}d].$

Array I consisted of a single constantan wire held taut between the base and lid of the convection chamber, with copper wires soldered onto it at $z = -\frac{5}{12}d, 0, \frac{5}{12}d$. The wire used in this array was 0.12 mm diameter and was electrically insulated from the convecting fluid by a phenolic lacquer. Array II was made of 0.25 mm diameter constantan wire and 0.12 mm diameter copper wire so as to form a self supporting lattice and was electrically insulated from the convecting fluid by a phenolic lacquer. This was attached to a thin stainless steel tube (2 mm diameter) which passed through the acrylic lid and terminated at $z = \frac{3}{8}d$. Both arrays enabled the drift of wave patterns around the annulus to be monitored, but in particular, array I provided a measure of the vertical temperature gradient, and array II a measure of the vertical and horizontal temperature gradients.

(*d*) *Heat flow measurements*

The Nusselt number for the wall heated annulus with horizontal upper and lower boundaries is defined by $N = (\text{total rate of heat transfer}) \times \ln(b/a)/2\pi|T_b - T_a|\,d\bar{\kappa}$. The total heat transfer in the experiments was measured by the flow rates and changes in temperature of the water flowing into and out of the temperature baths. Allowance was made for the heat flow occurring when there was no convecting fluid by means of a null experiment. The accuracy of the resulting Nusselt number measurements is estimated to be ± 1.5. This large error is due to the apparatus not being specifically designed for such measurements.

(*e*) *Flow visualization*

In the experiments with a free upper surface, streak photography of aluminium particles floating on the upper surface was used to identify wave numbers and flow types. In experiments with a rigid upper surface this technique is precluded and to enable the form of the flow to be seen, a horizontal flat beam of light was shone into the convection chamber at $z = 0$ through the clear acrylic ring in the outer cylinder (see figure 23). The flat beam was obtained by collimating the light from three 30 W single filament strip lights mounted in the form of a horizontal triangle. The collimating slits were 0.5 cm wide. The heating of the fluid by the lamps when they were switched on was less than 0.17 J s^{-1} and therefore negligibly small compared with the typical rate of heat transfer in the annulus of 50 J s^{-1}. With water as a working fluid a small amount of

aluminium powder suspension was added to the convecting fluid. The flakes which form this powder aline themselves with the flow and indicate the structure of the waves. With a glycerol–water solution as a working fluid it was possible to choose the density of the solution so that polystyrene beads were neutrally buoyant. These beads are 0.5 mm in diameter and translucent so that a streak photograph of their motions may be taken.

With both of these methods of flow visualization short sequences of ciné film were taken for each experiment so that the flow types could be clearly identified. The ciné camera, like the 35 mm camera used to take stills and streak photographs, was mounted on a tripod attached to the turntable, at a height of 1 m above the top of the convection chamber with its lens centred on the axis of rotation. With the camera in this position, a region of the convection chamber near the inner cylinder, especially at the bottom of the chamber, would normally be outside its field of view, being obscured by the top of the inner cylinder. The conical clear acrylic lid to the convection chamber acts as a lens and depending on the sign of the lower slope may diminish or increase this effect. Thus not only were the lower surfaces of the lids sloped, but the upper surface for each lid was also made conical at such an angle that this obscuring effect was removed (see figure 23).

(*f*) *Experimental procedure*

The procedure for making each experimental run consisted of: (i) setting the angular speed of the turntable and temperatures of the baths to predetermined values; (ii) waiting until it seemed from the readings of the thermocouples immersed in the fluid that transient phenomena associated with the setting up processes had disappeared; (iii) waiting a further interval of about three times the previous interval (amounting to about 2 h when $(T_b - T_a) \approx 10\,\mathrm{K}$ and 3 h when $(T_b - T_a) \approx 3\,\mathrm{K}$); and (iv) then carrying out the various measurements required.

4. Experimental results

(*a*) *The internal temperature structure*

In the linear theory the slope of the isotherms of the basic state was imposed, but in the experiments the slope is determined by convection and changes not only with external parameters, but also according to the type of flow. The isotherm slope plays a fundamental role in the theory, so, before the experimental results relating to the theory are presented, we first consider how the isotherm slope varies in the experiments.

(i) *Method of measurement*

Thermocouple array II, which was described in § 3 gives a measure of the slope of the isotherms in the interior of the fluid. This array was seen to produce significant distortions in the wave patterns and to cause a reduction in the value of Θ at the upper symmetric transition, of about 20 %. The much smaller thermocouple array I, produced only very slight distortions in the wave patterns, and any changes in the upper symmetric transitions were less than 10 % of Θ. In order to avoid the distortions produced by array II, array I was used in the majority of the experiments and in consequence the isotherm slope was not generally measured. The slopes of the isotherms were, however, measured by using array II in a limited number of experiments to assist in the interpretation of the data obtained by using array I. The results presented here are for boundary slopes of magnitude 12°. In experiments with boundary slopes of magnitude 36° geometric restrictions limited the size of array II so that it sampled only the central one-third of the fluid.

PHILOSOPHICAL TRANSACTIONS OF THE ROYAL SOCIETY A MATHEMATICAL, PHYSICAL & ENGINEERING SCIENCES

The results with 36° slopes were consequently less meaningful, but showed good qualitative agreement with the results with 12° slopes. Owing to errors in measuring the temperatures and spatial coordinates of the array, the determinations of the mean isotherm slope ζ, have an estimated error of $\pm 7°$. In all the measurements it was found that the value of the slope of the isotherms over array II varied considerably, by typically 100 % of the mean slope of the isotherms over the array.

TABLE 2. EXPERIMENTAL DETERMINATIONS OF $I = \zeta \operatorname{sgn}(T_a - T_b)$ AND σ_z AT DIFFERENT VALUES OF Ω FOR $Q_1 = Q_u = 0$ (LIQUID USED: WATER, $a = 3.80$ cm, $b = 8.43$ cm, $d = 12$ cm)

	$T_b - T_a \approx 10$ K		$T_b - T_a \approx -10$ K	
Ω/rad s^{-1}	I/deg	σ_z	I/deg	σ_z
	rigid upper surface			
0 †	−9	0.77	9	0.65
0.27†	6	0.79	20	0.69
0.52†	20	0.83	31	0.76
0.99	23	0.84	33	0.78
1.92	22	0.86	29	0.81
3.90	18	0.88	28	0.90
	free upper surface			
0 †	−5	0.75	9	0.63
0.27†	15	0.79	21	0.70
0.52†	29	0.86	37	0.89
0.99	30	0.85	38	0.80
1.92	23	0.81	25	0.84
3.90	17	0.86	17	0.85

† Symmetric flow present in the annulus.

(ii) $\theta_1 = \theta_u = 0$

The present results for $\theta_1 = \theta_u = 0$ (table 2) agree qualitatively with the previous work of Smith (1958), Bowden & Eden (1965), Ketchum (1972) and Kaiser (1969). As Ω increases the slope of the isotherms multiplied by the sign of $(T_a - T_b)$ i.e. $I = \zeta \operatorname{sgn}(T_a - T_b)$ (this is a positive quantity when the sign of $\partial T/\partial r$ in the interior of the fluid is the same as that of the applied radial temperature difference $(T_b - T_a)$), increases from a small value greater or less than zero at $\Omega = 0$ to a maximum of about 30° just before the wave flow occurs. Then, after a sharp decrease, a further decrease with increasing Ω occurs.

Though not clear from table 2, I increases slowly with increasing Ω in the irregular régime (Ketchum 1972). Quantitative agreement with the previous work is precluded by the differences in geometry. In agreement with the previous work I is generally less with a rigid upper surface. In so much as the increase in I with Ω in the symmetric flow is probably due to the decreasing flux in the Ekman layers (see § 4 (*a*) (iii) below), the increase in I with a free upper surface may be due to the reduced mass flux in the free surface boundary layer. The differences between the $(T_b - T_a) > 0$ and $(T_b - T_a) < 0$ which occur even when $\Omega = 0$ are most likely to be due to curvature effects and variations of the properties of the fluid with temperature. The decrease in I in the wave régime is probably due to the radial transports of heat effected by the waves. The increase in I in the irregular régime may correspondingly be due to the reduced efficiency of the radial heat transport, as indicated by the drop in heat transfer in this régime.

(iii) *The effect of* $\theta_1 \neq 0$, $\theta_u \neq 0$ *on* I: *some expectations*

When, as in the present experiments, the thermal Rossby number Θ is $O(1)$ and the Ekman number $\mathscr{E} \ll 1$ the theory of McIntyre (1968) is appropriate. The meridional flux is controlled by the Ekman layers on the upper and lower boundaries whereas the side wall boundary layers are dominated by convection and their thickness is independent of rotation. As the rotation rate is increased the Ekman layer flux decreases and by continuity so does that of the side wall boundary layers. Thus fluid parcels in the side wall boundary layers have more time to gain or lose heat and the vertical temperature gradients in these layers become concentrated in the 'starting corners' at the top of the cold wall and the bottom of the hot wall. The isotherms slope across the interior of the fluid between the corresponding temperatures on the side wall boundary layers. Thus, if for example the depth of the annulus is increased, the vertical separation of the starting corners and hence the slope of the isotherms is increased. If the upper and lower boundaries are allowed to slope parallel to each other in the $Q_l = Q_u > 0$ case, the starting corners are moved vertically further apart and hence a corresponding increase in I is expected. In the $Q_l = Q_u < 0$ case, the starting corners are moved vertically nearer and hence a 'geometric' decrease in I is expected.

(iv) $\theta_l = \theta_u \neq 0$

The experimentally observed values of I and ΔI (ΔI is the difference in I between this experiment and another one, identical except that $\theta_l = \theta_u = 0$) for the $Q_l = Q_u > 0$ and $Q_l = Q_u < 0$ cases are given in table 3. When the flow is symmetric the geometrically expected changes in I are seen. In the wave régime for $Q_l = Q_u > 0$, a decrease in I with increasing Ω occurs; this is probably due to the radial transports of heat effected by the waves. However, in the wave régime for $Q_l = Q_u < 0$ I increases with Ω; this is accompanied by a decrease in heat flow, and may be explained by the reduced efficiency of the waves in transporting heat (see § 4 (*e*)). In as much as the linear theory growth rates can be associated with the heat transfer of the fully developed waves, these results are in keeping with the theoretically increased growth rates for $Q_l = Q_u > 0$ and the decreased growth rates for $Q_l = Q_u < 0$ (see figures 7 and 8).

TABLE 3. EXPERIMENTAL DETERMINATIONS OF $I = \zeta \operatorname{sgn}(T_a - T_b)$, ΔI (ΔI IS THE DIFFERENCE IN I BETWEEN THIS EXPERIMENT AND ANOTHER ONE, IDENTICAL EXCEPT THAT $\theta_l = \theta_u = 0$) AND σ_z, AT DIFFERENT VALUES OF Ω FOR $\theta_l = \theta_u = -12°$, I.E. $Q_l = Q_u > 0$ ($(T_b - T_a) > 0$) AND $Q_l = Q_u < 0$ ($(T_b - T_a) < 0$) (RIGID UPPER SURFACE; LIQUID USED: WATER; $a = 3.80$ cm, $b = 8.43$ cm, $d = 12$ cm)

	$T_b - T_a \approx 10$ K			$T_b - T_a \approx -10$ K		
Ω/rad s^{-1}	I/deg	ΔI/deg	σ_z	I/deg	ΔI/deg	σ_z
0 †	6	15	0.67	−9	−18	0.77
0.27†	24	18	0.71	1	−19	0.79
0.52†	37	17	0.76	15	−17	0.82
0.99	43	20	0.83	16	−17	0.84
1.92	34	12	0.87	28	−1	0.90
3.90	15	−3	0.85	49	21	0.95

† Symmetric flow present in the annulus.

(v) $\theta_l = -\theta_u$

In the $Q_l = -Q_u$ case no geometric changes in the isotherm slopes are expected, as no changes in the vertical separation of the starting corners occur. Table 4 shows the results for this case; the changes in the symmetric régime show that effects other than the geometric one discussed here, are occurring. The subsequent increase in I with Ω in the wave régime is in keeping with the observed reduction in heat transfer and the reduced growth rates in the theory.

TABLE 4. EXPERIMENTAL DETERMINATIONS OF $I = \zeta \mathrm{sgn}(T_a - T_b)$, ΔI (ΔI IS THE DIFFERENCE IN I BETWEEN THIS EXPERIMENT AND ANOTHER ONE, IDENTICAL EXCEPT THAT $\theta_l = \theta_u = 0$) AND σ_z, AT DIFFERENT VALUES OF Ω FOR $\theta_l = -\theta_u = 12°$, I.E. $Q_l = -Q_u > 0$ ($(T_b - T_a) < 0$) AND $Q_l = -Q_u < 0$ ($(T_b - T_a) > 0$) (RIGID UPPER SURFACE; LIQUID USED: WATER; $a = 3.80$ cm, $b = 8.43$ cm, $d = 12$ cm)

	$T_b - T_a \approx 10$ K			$T_b - T_a \approx -10$ K		
Ω/rad s^{-1}	I/deg	ΔI/deg	σ_z	I/deg	ΔI/deg	σ_z
0 †	−3	7	0.59	−1	−10	0.58
0.27†	11	8	0.64	12	−8	0.63
0.52†	25	8	0.70	25	−6	0.71
0.99	28	12	0.77	28	−5	0.79
1.92	36	14	0.75	30	1	0.85
3.90	36	18	0.80	42	14	0.89

† Symmetric flow present in the annulus.

(vi) $\theta_l \neq 0$, $\theta_u = 0$

If only the lower boundary slopes ($Q_u = 0$), then a 'geometric' increase in I is expected for $Q_l > 0$ and a decrease for $Q_l < 0$. Table 5 shows the experimental results for the case with a free upper surface and a sloping lower surface. In the symmetric régime I is seen to change in accordance with the geometric expectations. In the wave régime, in the $Q_l > 0$ case, I increases only slightly more. This is in keeping with the small difference in the heat transfer and theoretical growth rates from those in the $Q_l = Q_u = 0$ case. In the $Q_l < 0$ case, however, I increases appreciably in the wave régime. This corresponds with the observed reduction in heat transfer and the reduced growth rates in the theory.

TABLE 5. EXPERIMENTAL DETERMINATIONS OF $I = \zeta \mathrm{sgn}(T_a - T_b)$, ΔI (ΔI IS THE DIFFERENCE IN I BETWEEN THIS EXPERIMENT AND ANOTHER ONE, IDENTICAL EXCEPT THAT $\theta_l = \theta_u = 0$) AND σ_z, AT DIFFERENT VALUES OF Ω FOR $\theta_l = -12°$ AND $\theta_u \approx 0$ (UPPER SURFACE FREE), I.E. $Q_l > 0$ ($(T_b - T_a) > 0$) AND $Q_l < 0$ ($(T_b - T_a) < 0$) (FREE UPPER SURFACE; LIQUID USED: WATER; $a = 3.80$ cm, $b = 8.43$ cm, $d = 12$ cm)

	$T_b - T_a \approx 10$ K			$T_b - T_a \approx -10$ K		
Ω/rad s^{-1}	I/deg	ΔI/deg	σ_z	I/deg	ΔI/deg	σ_z
0 †	0	5	0.60	0	−8	0.65
0.27†	25	10	0.67	8	−13	0.75
0.52†	39	10	0.79	21	−17	0.90
0.99	43	13	0.83	22	−16	0.81
1.91	35	11	0.81	27	2	0.83
3.90	35	17	0.82	41	24	0.87

† Symmetric flow present in the annulus.

PHILOSOPHICAL TRANSACTIONS OF THE ROYAL SOCIETY A MATHEMATICAL, PHYSICAL & ENGINEERING SCIENCES

(vii) *The effect of sloping boundaries on the vertical stratification*

It is useful to introduce, following Hide (1967), an internal dimensionless parameter σ_z which measures the vertical temperature gradient. σ_z is defined as the spatially averaged value of the vertical temperature gradient $\partial T/\partial z$ divided by $|T_b - T_a|/d$. σ_z was measured by linear extrapolation of the temperatures measured with array II. These determinations have a relative accuracy of ± 0.04 due to errors in measuring the the temperatures and spatial coordinates of the array. The absolute accuracy, if some account is taken of possible variations of $\partial T/\partial z$ outside the array and vertical variations of the temperatures of the side walls, is about ± 0.1. For $0.5 < \Omega/\mathrm{rad\,s^{-1}} < 5$ and the whole range of slope configurations considered, σ_z remains nearly constant at 0.82 ± 0.13. Values of σ_z for the various 12° experimental cases are given in tables 2–5 and may be compared with the values of I. The small changes in σ_z which occur with variations of both Ω and the slopes do not always reflect the changes seen in I. This seems to be a consequence of the marked variability of $\partial T/\partial r$ and $\partial T/\partial z$ in the interior of the fluid.

(*b*) *The transition from axisymmetric to non-axisymmetric flow*

(i) *Method of measurement*

B_c, the value of B at the upper symmetric transition, was found by making experimental runs, as described in § 3 (*f*), in which only Ω was varied and all other experimental variables were held constant. Ω was systematically varied until the highest value of B at which waves occurred was within about 5 % of the lowest value of B at which symmetric flow occurred. B_c was then taken as the arithmetic mean of these two values of B. The reproducibility of the transitions measured in this way was found to be within ± 8 % of B_c. The absolute accuracy of the measurements, when allowance is made for the errors in the various parameters which comprise B, is about ± 20 % of B_c.

The exact nature of the transition was found to vary in the experiments, mainly between experiments with a rigid upper surface and those with a free upper surface. Table 6 shows typical experimental data used to determine the upper symmetric transition. ΔT_m is the peak to peak amplitude of the temperature fluctuations at $r = \frac{1}{2}(a+b)$, $z = 0$. This was measured by amplifying the voltage from a thermocouple in this position and displaying the result on a chart recorder. The values of $\Delta T_m/|T_b - T_a|$ up to about 0.005 can be attributed to various sources of electrical noise in the environment of the experiments, and values of 0.001 were obtained on occasions when this noise was at a minimum. Because of this background noise the wave flows were arbitrarily defined as occurring when $\Delta T_m/|T_b - T_a| \geqslant 0.01$. Waves were not seen by the methods of flow visualization used until $\Delta T_m/|T_b - T_a| \gtrsim 0.04$. The difference between the transition as judged by eye and that by ΔT_m was not more than about 10 % of B_c. The rate of decrease of ΔT_m as the transition is approached from the wave side, both in the present experiments and in those of Pfeffer, Fowlis, Fein & Buckley (1970) and Kaiser (1970), suggests that $\Delta T_m/|T_b - T_a|$ does go to zero close to where it has decreased to a value of 0.01, and that this criterion is therefore suitable.

The data in table 6 (*a*) is typical of all the experiments with a rigid lid. As B is decreased $\Delta T_m/|T_b - T_a|$ is seen to steadily build up from zero to a value of 0.25. The Nusselt numbers show no detectable changes while the waves build up and similarly σ_z seems to increase steadily in spite of the build up of the waves.

Table 6 (*b*) shows results typical of experiments with a free upper surface. The heat transfer decreases steadily in the symmetric flow, and shows no change when the 'small waves' not visible to the eye occur. The change to 'large waves' visible to the eye occurs abruptly (as previously noted by Kaiser 1970) and there is associated with this change an increase of 20 % in the Nusselt numbers. The vertical stability as measured by σ_z takes the high value of 0.99 (note the probable 5 % overestimate of σ_z due to vertical variations of temperature in the side walls) in the symmetric flow, and only when the 'large waves' visible to the eye occur does it decrease by about 15 %.

Table 6 (*c*) shows data typical of a free surface case which has been stabilized by sloping the lower boundary. No small waves, detected only by thermocouple, were seen, but in view of the limited number of measurements this does not preclude their existence. The effect of the stabliza-

TABLE 6. TYPICAL EXPERIMENTAL DATA FOR DETERMINING THE UPPER SYMMETRIC TRANSITION (LIQUID USED: WATER; $a = 3.80$ cm, $b = 8.43$ cm, DEPTH AT $r = \frac{1}{2}(a+b) = 12$ cm)

Ω/rad s^{-1}	Θ	B	σ_z	N	$\Delta T_m/(T_b - T_a)$	flow type†
(*a*) $\theta_l = 36°$, $\theta_u = -36°$; rigid upper surface; $T_b - T_a \approx -10$ K						
0.504	4.30	0.904	0.84	9	0.004	s
0.640	2.74	0.587	0.86	8	0.005	s
0.700	2.25	0.484	0.86	9	0.005	s
0.720	2.14	0.487	0.91	9	0.005	s
0.740	2.02	0.467	0.91	9	0.006	s
0.753	1.92	0.429	0.90	8	0.009	saw
0.775	1.86	0.417	0.90	8	0.025	saw
0.799	1.79	0.398	0.89	8	0.037	w
0.869	1.50	0.336	0.90	8	0.058	w
0.989	1.14	0.262	0.93	8	0.203	w
1.44	0.543	0.128	0.94	8	0.268	w
(*b*) $\theta_l = 0$, $\theta_u \approx 0$; free upper surface; $T_b - T_a \approx -10$ K						
0.495	4.78	1.06	0.89	7	0.002	s
0.749	2.16	0.535	0.99	6	0.001	s
0.753	2.15	0.533	0.99	6	0.003	s
0.759	2.12	0.528	0.99	6	0.009	saw
0.771	2.06	0.512	0.99	5	0.012	saw
0.790	1.97	0.488	0.99	5	0.015	saw
0.853	1.64	0.349	0.85	7	0.186	w
0.946	1.33	0.266	0.80	7	0.246	w
1.44	0.565	0.115	0.81	7	0.345	w
(*c*) $\theta_l = -36°$, $\theta_u \approx 0$; free upper surface; $T_b - T_a \approx -10$ K						
0.507	4.72	1.16	0.98	7	0.002	s
0.757	2.19	0.539	0.98	6	0.002	s
0.813	1.91	0.503	0.99	5	0.002	s
0.815	1.81	0.391	0.87	7	0.278	w
0.836	1.73	0.379	0.88	7	0.259	w
0.845	1.79	0.465	0.99	5	0.002	s
0.846	1.68	0.369	0.88	7	0.251	w
0.858	1.64	0.367	0.90	7	0.259	w
0.873	1.68	0.436	0.99	4	0.002	s
0.873	1.58	0.355	0.90	7	0.264	w
0.878	1.67	0.434	0.99	4	0.002	s
0.895	1.49	0.334	0.90	8	0.264	w
0.919	1.42	0.312	0.88	7	0.271	w
0.975	1.27	0.272	0.86	8	0.269	w
1.43	0.592	0.130	0.88	7	0.189	w

† See table 15 for key to flow types.

PHILOSOPHICAL TRANSACTIONS OF THE ROYAL SOCIETY A MATHEMATICAL, PHYSICAL & ENGINEERING SCIENCES

tion is to allow the symmetric flow to occur for higher values of Ω. The Nusselt numbers which decrease with increasing Ω in the symmetric régime correspondingly reach the smaller value of 4 before the wave flow occurs. When the wave flow occurs the Nusselt number increases suddenly to 7, and as before σ_z decreases. This large change in N and σ_z at the transition reflects large changes in the internal temperature structure which cause a hysteresis effect: for some values of the external parameters Θ and Ω the flow type is not unique.

TABLE 7. VALUES OF B AT THE UPPER SYMMETRIC TRANSITION FOR PARALLEL UPPER AND LOWER BOUNDARIES, I.E. $\theta_1 = \theta_u$ ($a = 3.80$ cm, $b = 8.43$ cm, DEPTH AT $r = \frac{1}{2}(a+b) = 12$ cm)

		$\lvert\theta_1\rvert$/deg × sgn Q_1				
liquid used†	$(T_b - T_a)$/K	−36	−12	0	12	36
water	10	—	0.57	0.63	0.56	0.38
water	−10	0.09‡	0.50	0.56	0.46	—
water–glycerol solution	3	—	0.33	0.36	0.34	0.29
water–glycerol solution	−3	S§	0.28‡	0.29	0.29	—

† See table 1 for the properties of the liquids.
‡ Lower transition falls within the range of experiments, i.e. at $B = 0.029$ for the −36 case, and at $B = 0.0075$ for the −12 case.
§ No wave regime occurred.

(ii) *Results*

(1) $\theta_1 = \theta_u$. Table 7 shows values of B_c at the upper symmetric transition for parallel upper and lower boundary caes, i.e. $\theta_1 = \theta_u$. The results for $Q_1 = Q_u > 0$ should be compared with figure 24A which shows, on a B against $|\theta_1|$ graph, marginal stability envelopes for this case. The marginal stability curves are drawn for three different values of isotherm slope (15°, 33°, 60°) for conditions which are otherwise very similar to those in the experiments with $|T_b - T_a| \approx 10$ K (see legend). If the isotherm slopes at the transition were to remain unaltered when the boundaries are sloped then the curve for $I = 33°$ ($\sigma_z = 0.8$) would be appropriate for all the data. The increase, in this case, of the isotherm slope at the upper transition (see table 3) means that curves between $I = 33°$ and 60° are appropriate for the experimental data. The values of isotherm slope required to give agreement between theory and experiments as good as in the $\theta_1 = \theta_u = 0$ case, i.e. ± 20 % of B, have been calculated and compared with the corresponding values of isotherm slope measured in the experiments. It has been found that the calculated values of isotherm slope are within ± 10° of the measured slopes. Considering the error in measuring the slope with array II is ± 7° and the variability of the slope over the array alone is about ± 100 % this degree of agreement is as good as could be hoped for. It appears that, to within bounds no larger than ± 20 % of B_c and ± 10° of the isotherm slope, there is quantitative agreement with theory.

In the $Q_1 = Q_u < 0$ case the results in table 7 also show a stabilization, and in the case of 36° slopes it is very marked giving a complete stabilization in the 3 K case. At first sight this stabilization appears to be contrary to theoretical expectations of a destabilization. However, the measurements of isotherm slopes at the transition show them to be decreased by these boundary slopes. This reduces the growth rates of the waves and makes viscous damping so important as to account for the stabilization. Figure 24B shows theoretical marginal stability curves for isotherm slopes of 15°, 33° and 60° for the $Q_1 = Q_u < 0$ case. From these curves it is evident that the decrease in isotherm slope easily accounts for the observed stabilization. As in the $Q_1 = Q_u > 0$ case, when a detailed comparison is made it is found that, to within 20 % of B_c and ± 10° of the

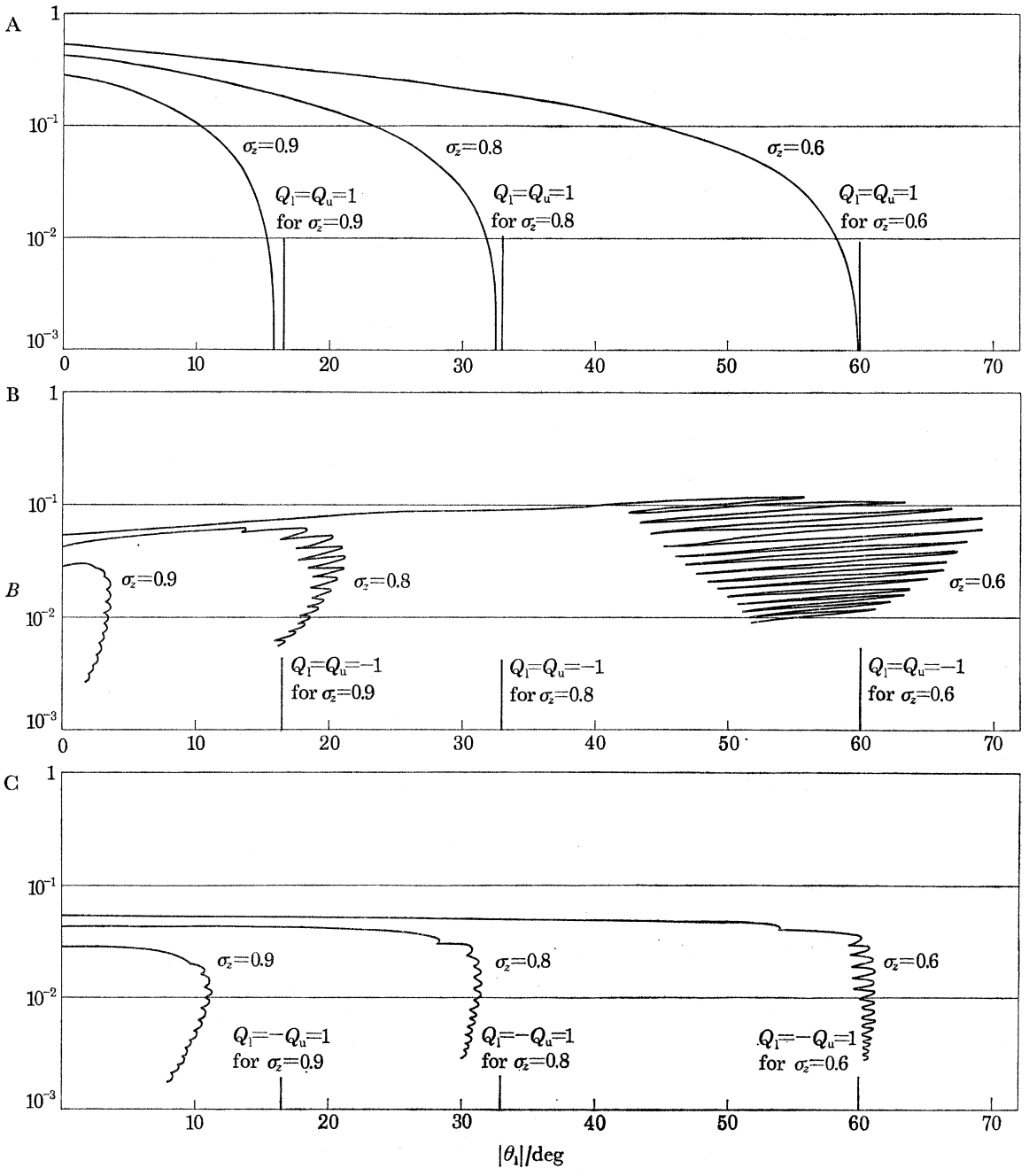

FIGURE 24. Illustrating the dependence of marginal stability curves on the slope of the isotherms for A; $Q = Q_u > 0$. B; $Q_l = Q_u < 0$. C; $Q_l = -Q_u$. The calculations are based on the extension of Eady's (1949) theory of baroclinic instability to include the effects of both Ekman layers and sloping upper and lower boundaries (Hide 1969). The marginal stability curves for 3 values of isotherm slope (nominally 15°, 33° and 60°) corresponding to $\sigma_z = 0.9$, 0.8 and 0.6 with $\sigma_r = 1 - \sigma_z$ are drawn on a B against $|\theta_l|$ graph. The variables are Q_l and Ω. The fixed parameters are $a = 3.80$ cm, $b = 8.43$ cm, $d = 12$ cm, $\bar{\rho} = 1\,\mathrm{g\,cm^{-3}}$, $\bar{\nu} = 0.01\,\mathrm{cm^2\,s^{-1}}$, $\partial|\rho|/\partial z| = |\Delta\rho|\sigma_z/d$ and $|\partial\rho/\partial r| = |\Delta\rho|\,\sigma_r/(b-a)$ where $|\Delta\rho| = 2\times10^{-3}\,\mathrm{g\,cm^{-3}}$.

isotherm slope, quantitative agreement is obtained. In two of these $Q_l = Q_u < 0$ cases as indicated in table 7 a lower transition has been found and measured. This is in agreement with the expected stabilization of the lower symmetric transition and quantitative agreement with theory to within $\pm 10°$ of the slope of the isotherm is obtained.

TABLE 8. VALUES OF B AT THE UPPER SYMMETRIC TRANSITION FOR OPPOSITELY SLOPING UPPER AND LOWER BOUNDARIES, I.E. $\theta_l = -\theta_u$ ($a = 3.80$ cm, $b = 8.43$ cm, DEPTH AT $r = \frac{1}{2}(a+b) = 12$ cm)

		θ_l/deg				
liquid used†	$(T_b - T_a)$/K	−36	−12	0	12	36
water	10	0.54	—	0.64	0.40	0.49
water	−10	0.42	—	0.57	0.45	0.45
water–glycerol solution	3	—	—	0.37	0.24	0.29
water–glycerol solution	−3	—	—	0.29	0.25	0.26

† See table 1 for the properties of the liquids.

(2) $\theta_l = -\theta_u$. Table 8 shows the results for the case when $\theta_l = -\theta_u$; here, as in case (1) ($\theta_l = \theta_u$), the flow is always found to be stabilized by the sloping end-walls, in qualitative agreement with the theoretical results expressed in figure 24C. So far as quantitative agreement is concerned this amounts to $\pm 20\,\%$ of B_c and $\pm 10°$ of the slope of the isotherms, which is comparable with (1).

TABLE 9. VALUES OF B AT THE UPPER SYMMETRIC TRANSITION FOR SLOPING LOWER BOUNDARIES WITH FREE OR HORIZONTAL RIGID UPPER BOUNDARIES ($a = 3.80$ cm, $b = 8.43$, DEPTH AT $r = \frac{1}{2}(a+b) = 12$ cm, LIQUID USED: WATER)

		$\lvert\theta_l\rvert$/deg × sgn Q_l				
upper surface	$(T_b - T_a)$/K	−36	−12	0	12	36
rigid	10	—	—	0.63	0.61	0.43
rigid	−10	0.43	0.56	0.56	—	—
free	10	0.23	0.35	0.48	0.40	0.41
free	−10	0.40	0.51	0.52	0.48	0.47

(3) $\theta_l \neq 0$, $\theta_u = 0$. Table 9 shows the results for experiments in which only the lower surface is sloped. Theoretically, effects such as in the $\theta_l = \theta_u$ cases are expected, and correspondingly the effects observed are similar to these in the $\theta_l = \theta_u$ experiments. A detailed comparison between theory and experiments for this case finds quantitative agreement to within $\pm 20\,\%$ of B_c and $\pm 10°$ of the slope of the isotherms, as in the previous cases.

(4) $\theta_l = \theta_u = 0$; *some lower symmetric transition data*. The results shown in table 10 are taken from the work of Douglas & Mason (1973) and are lower symmetric transition measurements in a large fluid annulus with $(b-a) = 15.34$ cm and a rigid upper surface ($\theta_l = \theta_u = 0$). The lower symmetric transition is observed only for $T_b - T_a \approx -10$ K cf. $T_b - T_a \approx +10$ K. As explained in § 2 (*d*) (iii), within the context of the linear theory, the effect of the sloping geopotentials is equivalent to that of allowing the upper and lower boundaries to slope in the opposite sense but same magnitude as the geopotential slope at $r = \frac{1}{2}(a+b)$. Thus the experimental lower transition data has been compared with the calculated lower transitions obtained by considering the effects of the geopotential slope. In Douglas & Mason's experiments the isotherm slopes were measured to an accuracy of $\pm 10\,\%$ and the measured values have been used to calculate the theoretical values of B_c. The agreement between the experimental and theoretical values of B at the transition (see table 10) is within $\pm 20\,\%$. This agreement is satisfactory considering the errors involved, and provide strong evidence that the sloping geopotentials have a strong influence on the lower symmetric transition. In the case when $T_b - T_a \approx +10$ K (i.e. $Q_u = Q_l > 0$), the effect of the geopotential slopes is to destabilize the lower symmetric transition, and in agreement with theoretical expectations this transition lay beyond the range of the experiments (see table 10).

PHILOSOPHICAL TRANSACTIONS OF THE ROYAL SOCIETY A MATHEMATICAL, PHYSICAL & ENGINEERING SCIENCES

TABLE 10. COMPARISON BETWEEN EXPERIMENTAL AND THEORETICAL VALUES OF B AT THE LOWER SYMMETRIC TRANSITION IN A LARGE ANNULUS WITH $\theta_1 = \theta_u = 0$ AND A RIGID UPPER SURFACE ($a = 23.10$ cm, $b = 38.44$ cm, LIQUID USED: WATER)

(In the theory identical parameters were used but the upper and lower boundaries were assumed to slope at the same magnitude but in the opposite sense to the geopotentials at $r = \frac{1}{2}(a+b)$.)

$(T_b - T_a)$/K	d/cm	$\mathscr{T}$	I/deg	$Q_1 = Q_u$	B (experimental)	B (theoretical)
−10	15.34	2.05×10^{10}	48	−0.30	1.7×10^{-3}	1.8×10^{-3}
	6	1.55×10^{10}	3.9	−0.18	2.2×10^{-3}	1.6×10^{-3}
	2	3.44×10^{10}	5.0	−0.07	1.8×10^{-4}	1.5×10^{-4}
10	15.34	$> 10^{10}$	> 48	> 0.30	$< 10^{-3}$	$< 10^{-3}$
	6	$> 10^{11}$	> 48	> 0.30	$< 10^{-3}$	$< 10^{-3}$
	2	$> 10^{11}$	> 42	> 0.26	$< 10^{-4}$	$< 10^{-4}$

(5) *Summary.* From both the present experiments and those of Douglas & Mason's it appears that, given the (experimentally-determined) slope of the isotherms in the interior of the fluid, the linear theory shows good agreement with the observed effects on the flow stability. To predict what effect particular boundary slopes have on the stability of the annulus system, it is also necessary to understand the non-linear processes which determine the slope of the isotherms. This difficult problem is not readily soluble and progress has been made only in special circumstances (see, for example, McIntyre 1968).

(c) *Wave numbers and flow types*

(i) *Method and measurement*

For all the slope configurations used in the experiments runs were made at a series of predetermined values of Ω. At each of these values of Ω the wave number and flow type were determined by examining short sequences of the ciné film. The results of this study of wave numbers and flow types are presented in tables 11–14. The various classifications and the key to the symbols used to denote them are given in table 15. It should be emphasized that this classification of flow types is both qualitative and subjective.

(ii) *Qualitative comparison with linear theory*

(1) $\theta_1 = \theta_u$. The results for the parallel rigid upper and lower boundary cases are given in table 11. The effects of the slopes on the wave numbers are in qualitative agreement with the theoretical expectations of § 2, i.e., an increase for $Q_1 = Q_u < 0$ and a decrease for $Q_1 = Q_u > 0$. The effect on the transition to the irregular flow is also very marked. Inspection of the $|\theta_1| = 12°$ data shows the irregular transition to occur at much lower Ω for $Q_1 = Q_u < 0$ and not to occur in the range of Ω considered for $Q_1 = Q_u > 0$.

It has been found empirically by Hide (1958) and confirmed by subsequent work (Fowlis & Hide 1965) that the wave numbers reach a maximum value m_{max} given by

$$0.7 \approx m_{max}(b-a)/\pi(b+a)$$

(implies $m_{max} \approx 5.8$ in the present experiments) just before the irregular flow occurs. The present experiments show that this approximate relation still holds, notwithstanding the sloping boundaries, provided that the waves extend across the full width of the annulus. Thus the changes in the irregular transition appear to correspond to the changes in the wave numbers.

TABLE 11. WAVE NUMBER AND FLOW TYPE DATA FOR RIGID PARALLEL UPPER AND LOWER BOUNDARIES (LIQUID USED: WATER, $a = 3.80$ cm, $b = 8.43$ cm, DEPTH AT $r = \frac{1}{2}(a+b) = 12$ cm, $|T_b - T_a| \approx 10$ K) (SEE TABLE 15 FOR THE KEY TO THE FLOW TYPES)

	$\lvert\theta_1\rvert$/deg × sgn Q_1							
		−12		0		12		
	−36							36
Ω/rad s^{-1}	$T_a > T_b$	$T_a > T_b$	$T_a < T_b$	$T_a > T_b$	$T_a < T_b$	$T_a > T_b$	$T_a < T_b$	$T_a < T_b$
0.8	s	4	3	2	2	2	1	1av
1.0	s	4	4	3	3	2	2av	1av
1.4	s	6	5	4	3	3	3av	2av, sv
1.9	saw	7ji	6	4ssv	4ssv	4	3	2av, sv
2.3	saw	7i	7ji	4sv	5ssv	4ssv	3	3lsv
2.7	saw	7vi	7i	5sv	5sv	4ssv	3ssv	3lsv
3.1	s	8vi	7i	5lsv	4sv	4sv	4sv	3lsv
3.4	s	9vi	7vi	5ji	4lsv	4lsv	4lsv	3lsv
3.9	s	10vi	7vi	6i	4ji	4lsv	4lsv	3lsv

TABLE 12. WAVE NUMBER AND FLOW TYPE DATA FOR OPPOSITELY SLOPING UPPER AND LOWER BOUNDARIES, I.E. $\theta_1 = -\theta_u$ (LIQUID USED: WATER, $a = 3.80$ cm, $b = 8.43$ cm, DEPTH AT $r = \frac{1}{2}(a+b) = 12$ cm, $|T_b - T_a| \approx 10$ K) (SEE TABLE 15 FOR THE KEY TO THE FLOW TYPES)

	θ_1/deg					
	0		−12		−36	
Ω/rad s^{-1}	$T_b > T_a$	$T_b < T_a$	$T_b > T_a$	$T_b < T_a$	$T_b > T_a$	$T_b < T_a$
0.8	2	2	2	2	1†	1†
1.0	3	3	3	3	2†	2av†
1.4	3	4	3, 6d	3	4†	4†
1.9	4ssv	4ssv	4d	4	5, 6ds	5, 6ds
2.3	5ssv	4sv	6	6	5, 8ds	6, 7ds
2.7	5sv	5sv	6d	6d, sv	6, 8ds	6, 9ds
3.1	4sv	5lsv	6ji	7i	7, 9ds	7, 10ds
3.4	4lsv	5ji	7i	7i	8, 9ds, ji	8, 10ds, ji
3.9	4ji	6i	7i	7i	9, 11ds, ji	9, 11ds, ji

† Waves do not extend across the annulus but remain close to the inner cylinder.

TABLE 13. WAVE NUMBER AND FLOW TYPE DATA FOR SLOPING LOWER BOUNDARIES WITH A HORIZONTAL RIGID UPPER BOUNDARY (LIQUID USED: WATER, $a = 3.80$ cm, $b = 8.43$ cm, DEPTH AT $r = \frac{1}{2}(a+b) = 12$ cm, $|T_b - T_a| \approx 10$ K) (SEE TABLE 15 FOR THE KEY TO THE FLOW TYPES)

	$\lvert\theta_1\rvert$/deg × sgn Q_1					
			0			
	−36	−12			12	36
Ω/rad s^{-1}	$T_a > T_b$	$T_a > T_b$	$T_a < T_b$	$T_a > T_b$	$T_a < T_b$	$T_a < T_b$
0.8	4	3	2	2	1	1
1.0	4	4av	3	3	2	1
1.4	6	4	3	4	3d	2, 1d
1.9	6, 8ds	6	4ssv	4ssv	5	4d, sv
2.3	6, 7ds	6sv	5ssv	4sv	5ssv	4d, sv
2.7	7ds	7ji	5sv	5sv	5sv	5d, sv
3.1	8ds	7i	4sv	5lsv	5sv	6ji
3.4	9ji	7i	4lsv	5ji	5lsv	7i
3.9	9i	7i	4ji	6i	6ji	7i

PHILOSOPHICAL TRANSACTIONS OF THE ROYAL SOCIETY A MATHEMATICAL, PHYSICAL & ENGINEERING SCIENCES

TABLE 14. WAVE NUMBER AND FLOW TYPE DATA FOR SLOPING LOWER BOUNDARIES WITH A FREE UPPER SURFACE (LIQUID USED: WATER, $a = 3.80$ cm, $b = 8.43$ cm, DEPTH AT $r = \frac{1}{2}(a+b) = 12$ cm, $|T_b - T_a| \approx 10$ K) (SEE TABLE 15 FOR THE KEY TO THE FLOW TYPES)

	$\lvert\theta_1\rvert$/deg × sgn Q_1									
	−36		−12		0		12		36	
Ω/rad s^{-1}	$T_a > T_b$	$T_a < T_b$	$T_a > T_b$	$T_a < T_b$	$T_a > T_b$	$T_a < T_b$	$T_a > T_b$	$T_a < T_b$	$T_a > T_b$	$T_a < T_b$
0.8	4	s	2	3	2	2	2av	2	s	s
1.0	4	3	2	3	3	3	3	3	2	2
1.4	6	6	4	4	4	3	3	4	3	3
1.9	7ji	6ji	5	5	4ssv	4ssv	5	4	4	4
2.3	8i	7i	6	5	4sv	5ssv	5	4	5	5
2.7	8i†	7i	7ji†	6	5sv	5sv	6	6	6av	6ji
3.1	10vi†	8i†	8i†	6ds	5lsv	4sv	6	6sv	6av	6i
3.4	10vi†	9vi†	9i†	6ji†	5lsv	4lsv	6sv	6sv	6i	6i
3.9	10vi†	10vi†	10i†	6ji†	6ji	4ji	6sv	6ji	7i	6i

† Waves do not extend across the annulus but stay close to the inner cylinder.

TABLE 15. KEY TO THE CLASSIFICATION OF FLOW TYPES

*m*vi	very irregular flow: eddies growing and decaying in a complex fashion, the flow has no obvious dominant wavenumber and *m* is an estimate of the average number of eddies present in the flow
*m*i	irregular flow: eddies growing and decaying, but the flow has an obvious dominant wave number *m*
*m*ji	just irregular flow: the flow consists of *m* lobes which are fluctuating in amplitude and shape aperiodically
*m*lsv	large 'wave shape' vacillation
*m*sv	'wave shape' vacillation
*m*ssv	small 'wave shape' vacillation
	all *m* wave lobes tilt to and fro periodically
*m*lav	large 'wave amplitude' vacillation
*m*av	'wave amplitude' vacillation
*m*sav	small 'wave amplitude' vacillation
	the amplitude of all *m* lobes varies periodically
m, *m*wnv	wave number vacillation: this is similar to the large 'wave amplitude' vacillation, in which the waves vary between apparently zero amplitude (symmetric flow) and large fully developed waves, except that the wave number of the fully developed waves changes periodically from cycle to cycle of the amplitude vacillation
m_d, *m*d	wave dispersion; two wave numbers are present and are drifting relative to each other; m_d is the wave number of the dominant wave and *m* that of the other; on some occasions one wave so dominated the flow that only m_d was measureable and for these cases '*m*d' is given
m_i, $m_o$ds	separate dispersing wave trains: one wave train near the inner cylinder with wave number m_i propagates relative to the other near the outer cylinder with wave number m_o; on some occasions the wave near the outer cylinder was so weak its wave number could not be measured and in these cases '$m_i$ds' is given
m	regular waves: wave number *m*
saw	small amplitude regular waves: not indicated by flow visualization and detected only by thermocouple; hence wave number not measured
s	axisymmetric flow

The small amplitude waves which do not extend across the annulus occur near the upper and lower symmetric transitions and, as we shall see later, they occur in most circumstances for large values of $|\partial d/\partial r|$. In these cases where the waves do not extend across the full width of the annulus, the maximum wave numbers are greater but equal to the closest integer to that value of *m* for which the radial extent of the wave ($< (b-a)$) is equal to *ca.* 0.7 times the wavelength.

The effect of the $\theta_1 = \theta_u$ slopes on vacillation is an increase in the frequency of occurrence of amplitude and wave shape vacillation in the $Q_1 = Q_u > 0$ cases.

It is of interest to note that the differences between the $\theta_1 = \theta_u = 0$ cases for $T_b - T_a < 0$ and $T_b - T_a > 0$ at high values of Ω are as would be expected from the sloping geopotentials producing $Q_1 = Q_u < 0$ and $Q_1 = Q_u > 0$ effects.

(2) $\theta_1 = -\theta_u$. Table 12 shows wave number and flow type data for oppositely sloping upper and lower boundaries. With the 12° slopes the wave numbers are slightly increased, and correspondingly the irregular transition occurs at lower values of Ω. The change of depth with radius in these experiments is similar to a β-effect and according to the linear theory it makes the waves propagate relative to the mean flow by an amount which depends on the wave number. The finite amplitude waves of the annulus are not sinusoidal but may in general be represented by a basic wave number and its harmonics. Thus the linear theory would lead one to expect the various harmonics to propagate at different speeds relative to the mean flow, i.e. to wave dispersion. In some of the experimental runs wave dispersion was seen, but in most of the experiments only a single regular wave was present. The occurrence, in the experiments, of regular waves shows that non-linear effects can in most, but not all, circumstances inhibit the dispersion of the linear theory.

In connexion with these observations it is of interest to note that wave dispersion can occur in the annulus with $\theta_1 = \theta_u = 0$ (e.g. Pfeffer & Fowlis 1968). A plausible explanation of this dispersion is the basic vorticity gradient of the flow ($\approx -\partial^2 u/\partial y^2$) which is also similar to a β-effect (see § 4 (*d*)).

For the 36° cases of oppositely sloping boundaries (table 12), at low values of Ω, regular waves occur which do not extend across the full width of the annulus but remain close to the inner cylinder. They remain close to the inner cylinder not only for $T_b - T_a < 0$ and $T_b - T_a > 0$ but also for $\partial d/\partial r < 0$ and $\partial d/\partial r > 0$; this suggests that curvature effects probably determine the position of the wave train. At higher values of Ω a transition in the flow type occurs and two regular waves of different wave number occur together, one dominating near the inner cylinder and the other near the outer cylinder. These waves propagate at different speeds relative to the annulus, and the resulting flow patterns, though complicated, repeat themselves at regular intervals. As Ω increases further the two wave trains become progressively smaller in radial extent until at the highest values of Ω irregularities start to occur. Figure 25 shows temperature traces from thermocouples located on a single azimuth, $z = 0$ and $r = \frac{1}{3}(2a+b)$, $\frac{1}{2}(a+b)$ and $\frac{1}{3}(2b+a)$. These clearly show the single regular wave at low Ω and the presence of two separate waves at high Ω.

This radial variation in azimuthal wave number in the regular wave régime is unique to the present experiments with large value of $\partial d/\partial r$. Apart from cases near marginal stability the only other cases which show a pronounced limitation of the radial extent of waves are the highly irregular flows. In these irregular flows the eddies have a marked limitation in radial extent only when sloping geopotentials or sloping boundaries have tended to promote higher wave numbers (cf. figure 25 and figure 5). The observed phenomena cannot be explained by the simple linear theory of § 2, in which the most rapidly growing mode always has the $n = 1$ radial structure. In the absence of another theory it may be worth noting that in both the experiments with $\partial d/\partial r \neq 0$ and those with parallel sloping boundaries which promote higher wave numbers, a long wave cut-off is present. In the case of the large values of $\partial d/\partial r$ the radial extent of the waves is indeed *ca.* $(u/\beta)^{\frac{1}{2}}$ (where u is a typical flow speed) the value of the long wave cut-off wavelength. The radial extent of waves in the irregular flow is difficult to measure but the observed values are roughly consistent with the wavelengths corresponding to the long wave cut-off. If the limitation

of radial extent is linked to the presence of a long wave cut-off then it is of interest that the large values of $\partial d/\partial r$ have the additional effect of promoting regular flows.

(3) $\theta_u = 0, \theta_1 \neq 0$. Table 13 shows wave number and flow type data for a horizontal rigid upper surface and a sloping lower surface. Table 14 shows wave number and flow type data for a free upper surface and sloping lower surface. In both these cases the main effect is seen to be the theoretically expected increases in wave number for $Q_1 < 0$ and decreases for $Q_1 > 0$.

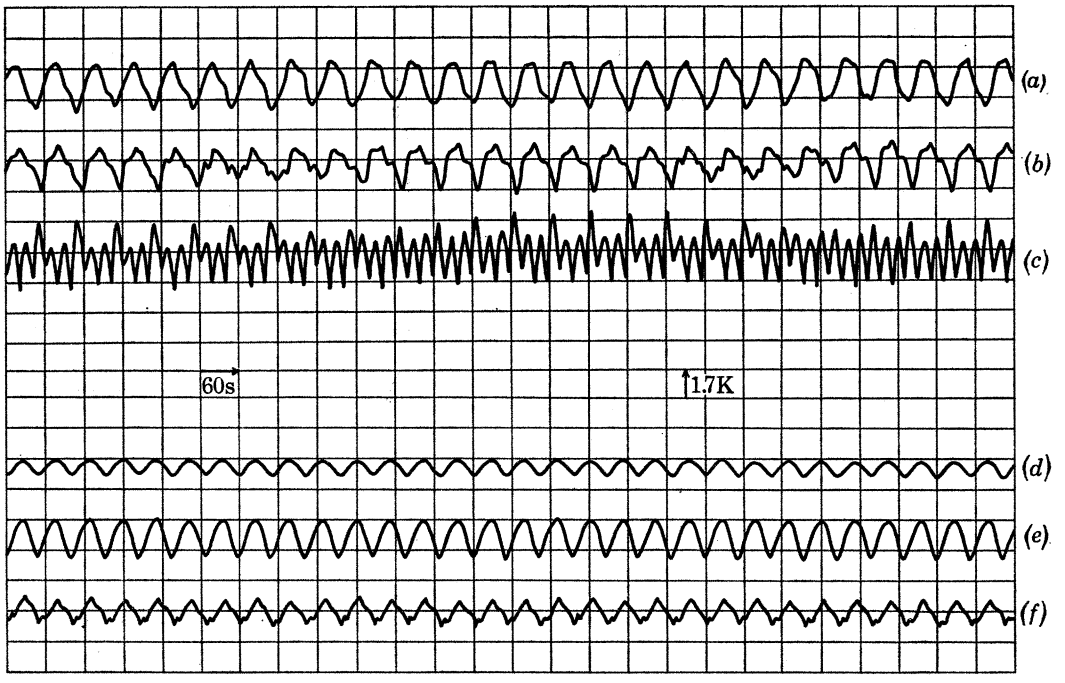

FIGURE 25. Temperature against time traces recorded by thermocouples at coordinates $(r, \phi, z) = [\frac{1}{3}(2a+b), 0, 0]$ (traces (*c*) and (*f*)), $[\frac{1}{2}(a+b), 0, 0]$ (traces (*b*) and (*e*)) and $[\frac{1}{3}(2b+a), 0, 0]$ (traces (*a*) and (*d*)). The traces illustrate flow types typical of boundaries sloping in opposite senses, i.e. $\theta_1 = -\theta_u = -36°$. Traces (*a*), (*b*) and (*c*) show separate wave trains near the inner and outer cylinders propagating at different speeds, and traces (*d*), (*e*) and (*f*) show a single regular wave. Other experimental details: $a = 3.80$ cm, $b = 8.43$ cm, $d = 12$ cm, liquid used water, $\bar{T} = 20.0\,°\text{C}$, $|\Delta\rho| = 2.03 \times 10^{-3}\,\text{g cm}^{-3}$, $T_a < T_b$, traces (*a*), (*b*) and (*c*) $\Omega = 2.76\,\text{rad s}^{-1}$, traces (*d*), (*e*) and (*f*) $\Omega = 1.45\,\text{rad s}^{-1}$.

(iii) *Quantitative comparison with theory.*

Having discussed qualitatively the wave number data for the cases in tables 11–14 we find it convenient to make a quantitative comparison with theory for all the data together. This comparison only includes data for fully developed waves which extend across the annulus, and excludes irregular flows and flows with two separate wave trains.

For fixed experimental conditions and $\theta_1 = \theta_u = 0$ there is a statistical variability from experiment to experiment in the observed wave number, and for values of a, b and d similar to those in the present experiments, three wave numbers are in general possible at fixed experimental conditions (see Hide 1958). In order to compare the experimental wave numbers with the theoretical predictions, table 17 shows the frequency of occurrence of wave numbers in *all* the experiments for various values of theoretically predicted wave numbers of maximum growth rate. For comparison table 16 shows the frequency of occurrence of wave numbers in all the experiments at the values of Ω at which measurements were taken. It is seen that for a particular

theoretical wave number, up to three different wave numbers are observed (cf. 6 different wave-numbers for a particular value of Ω). This is exactly what would be found with the $\theta_l = \theta_u = 0$ data alone, so we conclude that although there is no quantitative agreement it is clear that the experimental departures from the predictions of linear theory are independent of the presence of sloping boundaries. In the cases where the waves have smaller amplitudes and do not extend across the annulus, as might be expected, the experimental wave numbers are higher and closer to the predictions of linear theory.

(*d*) *Wave drift rates*

Before discussing the experimental data, it is useful to consider the various processes which would be expected to make the waves drift relative to the annulus. These can be divided into two classes: (i) those which produce a net mean zonal flow in the annulus, and (ii) those which make the waves propagate relative to the mean zonal flow.

A net mean (vertically averaged) zonal flow can be produced by variations of the physical properties of the fluid with temperature, curvature effects, sloping geopotentials, divergent upper and lower boundaries, and, in particular, asymmetry between the upper and lower boundary conditions such as a free upper surface and rigid lower surface. Only in the absence of all these effects do symmetry considerations require the net zonal flow to be zero.

TABLE 16. FREQUENCY OF OCCURRENCE OF WAVE NUMBERS IN ALL THE EXPERIMENTS FOR VARIOUS VALUES OF Ω

	wave number						
Ω/rad s^{-1}	1	2	3	4	5	6	7
0.8	6	11	6	3			
1.0	2	8	13	6			
1.4		2	10	10	3	4	
1.9		1	1	10	6	5	2
2.3			2	7	7	6	3
2.7			2	2	5	7	3
3.1			1	3	3	4	
3.4			1	3	3	2	
3.9			1	2	2	1	

TABLE 17. FREQUENCY OF OCCURRENCE OF WAVE NUMBERS IN ALL THE EXPERIMENTS FOR VARIOUS THEORETICAL MODELS OF MAXIMUM GROWTH RATE (CALCULATED FOR SIMILAR CONDITIONS TO THE EXPERIMENTS BUT ASSUMING THE SLOPE OF THE ISOTHERMS IS 33°)

theoretical mode of maximum instability	experimental wave number						
	1	2	3	4	5	6	7
1	2	5					
2	3	6					
3		3	10				
4		2	6	1			
5		1	5	8			
6			6	9	2		
7				11	5		
8				4	2	4	
9				1	5	6	
10					3	9	1
11					3	4	
12						3	2

TABLE 18. INVERSE WAVE DRIFT PERIODS ($\mathscr{T}^{-1} \times 10^3$) FOR RIGID PARALLEL UPPER AND LOWER BOUNDARIES (LIQUID USED: WATER, $a = 3.80$ cm, $b = 8.43$ cm, $d = 12$ cm, $|T_b - T_a| \approx 10$ K)

	$\lvert\theta_1\rvert$/deg × sgn Q_1								
		−12		0		12			
	−36								36
Ω/rad s^{-1}	$T_a > T_b$	$T_a > T_b$	$T_a < T_b$	$T_a > T_b$	$T_a < T_b$	$T_a > T_b$	$T_a < T_b$		$T_a < T_b$
0.8	—	0.40	0.58	0.40	1.19	0.79	1.37		1.33
1.0	—	0.06	0.32	0.29	0.87	0.65	1.04		1.67
1.4	—	0.00	0.51	0.16	0.58	0.15	0.69		1.11
1.9	—	−0.26	0.71	0.08	0.60	−0.02	0.48		0.54
2.3	—	—	0.93	0.01	0.53	−0.04	0.43		0.44
2.7	—	—	—	−0.07	0.34	−0.04	0.29		0.27
3.1	—	—	—	−0.08	0.35	−0.04	0.22		0.23
3.4	—	—	—	−0.08	0.30	−0.05	0.20		0.21
3.9	—	—	—	—	0.27	0.05	0.15		0.25

With $\theta_1 = \theta_u$ the unstable waves of the linear theory have the property of moving with the mean zonal flow, but this need not be a property of the finite amplitude annulus waves. Any property which disturbs the symmetry of the annulus might make the waves drift relative to the mean flow. Effects which would be expected to be important are (i) those equivalent to the β-effect and, in the free surface case (ii) the marked asymmetry between the upper and lower boundary conditions.

The wave drift rates were determined in the course of the experiments either directly from the ciné films of the flow, or by using the temperature traces together with the wave number observations.

(i) *Rigid upper and lower boundaries with* $\partial d/\partial r = 0$

The wave drift rates for cases with rigid parallel upper and lower surfaces are given in table 18. It is seen that for $T_a < T_b$ the drift rates are always > 0, i.e. in the sense of the rotation, but for $T_b < T_a$ the sign of the drift rates changes from > 0 at low Ω to < 0 at high Ω. No qualitative effects are produced by sloping the boundaries but at low Ω the drift rates are algebraically increased for $Q_u = Q_1 > 0$ and decreased for $Q_1 = Q_u < 0$.

In these cases with a rigid upper surface, the two main contributions to the mean flow would be expected to be due to the curvature of the annulus and the variation of viscosity with temperature. The contribution due to curvature effects can be estimated from theory (McIntyre 1968) or numerical calculations (Williams 1967) and is found to be of the same order as the observed drift rates. The sign of this contribution is however independent of the sign of $T_b - T_a$. The viscous mean flow can be estimated by considering the balance of the meridional flux in the upper and lower Ekman boundary layers; it should be proportional to the 'thermal wind' (see equation (2.9)) and an order of magnitude estimate is comparable with the observed drift rates. The sign of this contribution is the same as the sign of $T_b - T_a$.

In these parallel rigid lid cases there is no change of depth with radius or asymmetry in the boundary conditions to make the linear theory waves drift relative to the mean flow. The mean value of the β-effect due to the horizontal vorticity gradient, i.e. mean value of $-\partial^2 u/\partial y^2$ for the velocity profiles of the annulus, would be expected to be typically the value corresponding to $u\alpha((b-a)^2/4 - y^2)\,(z - z_0)$, i.e. $\partial^2 u/\partial y^2 = -12\bar{u}/(b-a)^2$ where $\bar{u}$ is the mean zonal flow. In the present experiments the consequent drift rates

$$\text{(barotropic theory phase velocity} = -\beta[(b-a)^2 l^2/(l^2 + 4(b-a)^2)\,\pi^2],$$

where l is the wavelength and here $\beta = 12\bar{u}/(b-a)^2$) relative to the mean flow would be typically of similar magnitude but opposite direction to $\bar{u}$. This produces a difficulty in interpreting the results, as the vorticity gradient is sensitive to the exact shape of the velocity profiles, and changes in these profiles could produce changes in the drift rates comparable with the mean flow.

If changes in the vorticity gradients are ignored, the observed results can be qualitatively explained as being due to a combination of effects due to curvature (drift always > 0) and the variation of viscosity with temperature (drift $\gtrless 0$ according to $T_b - T_a \gtrless 0$). If this explanation is correct the variations of drift rates with Ω in the $T_b > T_a$ and $T_b < T_a$ cases implies the curvature effect is roughly proportional to Ω^{-1} and the viscous effect to $\Omega^{-\frac{1}{2}}$. Support for this explanation comes from Douglas, Hide & Mason (1972) who measured the zonal velocity at $z = 0$ in an annulus with a rigid lid and found the variations to be qualitatively the same as the drift rates in the present experiments. The parallel slopes would not be expected to change the drift rates directly, and it is of interest that the small algebraic increase in drift rates with increasing $Q_1 = Q_u$ corresponds to an increase in the slope of the isotherms (see § 4 (*a*)) and hence in the thermal wind.

(ii) *Rigid upper and lower boundaries with* $\partial d/\partial r \neq 0$

Table 19 A shows drift rates for oppositely sloping rigid upper and lower boundaries. The waves are made to drift in a negative sense at somewhat larger speeds than occurred with the parallel upper and lower boundaries. It is supposed that the drift rates seen in these cases consist of a drift due to the β-effect produced by the slopes, together with a drift due to causes discussed in relation to the parallel slope cases. The phase speeds relative to the mean flow expected in the linear theory have been calculated and compared with the experimental observations (see table 19 B). The calculations include the effect of Ekman layers on the upper and lower boundaries, and were for conditions similar to those in the experiments, except the slope of the isotherms was taken as 33°. A few of the modes seen in the experiments were found to be stable in the calculations and for these cases no comparison was made. This stability can be explained by the inaccuracy of assuming the slope of the isotherms was always 33°. The ratio of the theoretical drift rate to the experimental value was in almost all cases between 0.8 and 0.4.

Table 20 A shows experimental data for a rigid horizontal upper surface and sloping lower surface. The drift rates are seen to be similar in direction to those when both surfaces sloped oppositely but about half the size. A comparison with linear theory (table 20 B) shows agreement to the same degree as with oppositely sloping boundaries.

In view of the many inappropriate assumptions of the linear theory the agreement with the experimental results in the above cases is remarkably good.

The drift rates of unstable waves given by the inviscid linear theory of § 2 are larger than the drift rates obtained from simple barotropic theory

$$(\text{barotropic phase velocity} = -\beta[(b-a)^2 l^2/(l^2 + 4(b-a)^2)\pi^2],$$

where $\beta = -2\alpha\Omega/d$, α is the angle of divergence of the slopes and l is the wavelength). In fact the ratio of the phase velocity of the unstable baroclinic waves to the phase velocity of the barotropic waves is $\gamma \coth \gamma$ (see § 2 (*a*)) which for the experimental waves is typically *ca.* 1.3. The effect of including Ekman layer friction in the linear baroclinic theory is to reduce the phase velocities bringing them closer to those given by simple barotropic theory. The result of a comparison of barotropic drift rates with all the experimental data is that the agreement is as good as with the baroclinic theory.

PHILOSOPHICAL TRANSACTIONS OF THE ROYAL SOCIETY A MATHEMATICAL, PHYSICAL & ENGINEERING SCIENCES

TABLE 19A. INVERSE WAVE DRIFT PERIODS ($\mathscr{T}^{-1} \times 10^3$) FOR OPPOSITELY SLOPING UPPER AND LOWER BOUNDARIES (LIQUID USED: WATER, $a = 3.80$ cm, $b = 8.43$ cm, DEPTH AT $r = \frac{1}{2}(a+b) = 12$ cm, $|T_b - T_a| \approx 10$ K)

	θ_1/deg							
	0		−12		−36			
Ω/rad s^{-1}	$T_b > T_a$	$T_b < T_a$	$T_b > T_a$	$T_b < T_a$	$T_b > T_a$		T_b/T_a	
0.8	1.19	0.40	−0.67	−0.90	−5.55		−6.25	
1.0	0.87	0.29	−0.94	−1.42	−4.90		−5.21	
1.4	0.58	0.16	−1.40	−1.85	−4.08		−5.00	
1.9	0.60	0.08	−0.98	−1.47	−4.72†	−2.96‡	−5.91†	−3.75‡
2.3	0.53	0.01	−0.62	−1.49	−7.75†	−1.37‡	−7.46†	−3.31‡
2.7	0.34	−0.07	—	—	−8.40†	−1.73‡	−8.54†	−1.96‡
3.1	0.35	−0.08	—	—	−8.62†	−1.42‡	−8.33†	−1.68‡
3.4	0.30	−0.08	—	—	−8.19†	−1.64‡	−8.06†	−1.78‡
3.9	0.27	—	—	—	−7.35†	−1.04‡	—	—

† Wave near inner cylinder. ‡ Wave near outer cylinder.

TABLE 19B. COMPARISON OF EXPERIMENTAL DRIFT RATES WITH THEORY FOR OPPOSITELY SLOPING UPPER AND LOWER BOUNDARIES: THE DIFFERENCE IN DRIFT RATES BETWEEN AN EXPERIMENT WITH SLOPES AND A SIMILAR ONE AT THE SAME VALUE OF Ω WITH ZERO SLOPES DIVIDED BY THE THEORETICAL VALUE OF DRIFT RATE FOR THE SAME Ω AND WAVE NUMBER (CALCULATED FOR SIMILAR CONDITIONS TO THE EXPERIMENT BUT ASSUMING THE SLOPE OF THE ISOTHERMS IS 33°)

	θ_1/deg			
	−12		−36	
Ω/rad s^{-1}	$T_b > T_a$	$T_b < T_a$	$T_b > T_a$	$T_b < T_a$
0.8	0.63	0.44	0.65	0.66
1.0	0.67	0.64	0.61	0.58
1.4	0.74	0.75	0.73	0.81
1.9	0.77	0.75	—	—
2.3	0.65	0.84	—	—

TABLE 20A. INVERSE WAVE DRIFT PERIODS ($\mathscr{T}^{-1} \times 10^3$) FOR SLOPING LOWER BOUNDARIES WITH A HORIZONTAL RIGID UPPER BOUNDARY (LIQUID USED: WATER, $a = 3.80$ cm, $b = 8.43$ cm, DEPTH AT $r = \frac{1}{2}(a+b) = 12$ cm, $|T_b - T_a| \approx 10$ K)

	$\lvert\theta_1\rvert$ deg × sgn Q_1					
			0			
	−36	−12			12	36
Ω/rad s^{-1}	$T_a > T_b$	$T_a > T_b$	$T_a < T_b$	$T_a > T_b$	$T_a < T_b$	$T_a < T_b$
0.8	−1.52	−0.38	1.19	0.40	−0.06	−0.46
1.0	−1.75	−0.41	0.87	0.29	−0.06	−1.11
1.4	−1.85	−0.54	0.58	0.16	−0.32	−2.45
1.9	—	−0.30	0.60	0.08	−0.06	−1.04
2.3	—	−0.53	0.53	0.01	−0.09	−1.28
2.7	—	—	0.34	−0.07	−0.15	−0.90
3.1	—	—	0.35	−0.08	−0.18	—
3.4	—	—	0.30	−0.08	−0.32	—
3.9	—	—	0.27	—	—	—

TABLE 20B. COMPARISON OF EXPERIMENTAL DRIFT RATES WITH THEORY FOR SLOPING LOWER BOUNDARIES WITH A HORIZONTAL RIGID UPPER BOUNDARY: THE DIFFERENCE IN DRIFT RATES BETWEEN AN EXPERIMENT WITH SLOPES AND A SIMILAR ONE AT THE SAME VALUE OF Ω WITH ZERO SLOPES DIVIDED BY THE THEORETICAL VALUE OF DRIFT RATE FOR THE SAME Ω AND WAVE NUMBER (CALCULATED FOR SIMILAR CONDITIONS TO THE EXPERIMENTS BUT ASSUMING THE SLOPE OF THE ISOTHERMS IS 33°)

	$\lvert\theta_1\rvert$/deg × sgn Q_1			
	−36	−12	12	36
Ω/rad s^{-1}	$T_a > T_b$	$T_a > T_b$	$T_a < T_b$	$T_a < T_b$
0.8	0.51	0.59	0.83	—
1.0	—	0.59	0.62	0.43
1.4	—	—	0.64	0.61
1.9	—	—	0.57	0.39
2.3	—	—	0.52	0.41
2.7	—	—	0.37	0.33
3.1	—	—	0.38	—
3.4	—	—	0.44	—
3.9	—	—	—	—

(iii) *Free upper surface*

Table 21 A shows experimental results for sloping lower surfaces with a free upper surface. The drift rates with the lower surface horizontal are typically ten times larger than in the corresponding parallel rigid upper and lower boundary cases. This large difference is due to the mean flow generated by the asymmetry of the free upper surface. Consideration of the balancing of torques and mass fluxes in the annulus implies that the mean flow due to the free upper surface should be roughly proportional to the thermal wind. Consequently as with the rigid upper surface case, the mean flow should vary with the slope of the isotherms. The measurements of isotherm slope (§ 5 (*a*)) indicate that this effect will confuse the effect of sloping the lower boundary. Additionally a number of processes can give rise to significant drift rates relative to this mean flow.

(1) The asymmetry of the free surface itself will make the linear theory waves drift relative to the mean flow. A calculation for the conditions of the present experiments, based on a theory (Hide 1969) similar to that in § 2 (*a*) but with the upper surface taken as free, indicates drift rates, which depend on Ω and m, having a typical size $3 \times 10^{-4}\,\mathrm{s}^{-1}$ (inverse drift period) in the same direction as the thermal wind, i.e. same sign as $T_b - T_a$.

(2) The curvature of the free upper surface due to the sloping geopotentials will cause the waves to drift relative to the mean flow. The size of this phase speed can be estimated from barotropic theory and $\approx -\beta[(b-a)^2 l^2/(l^2 + 4(b-a)^2)\,\pi^2]$, where $\beta = -(a+b)\,\Omega^3/gd$, l is the wavelength, and the slope of the geopotentials at $r = \frac{1}{2}(a+b)$ has been considered. For the present data the largest drift rate from this effect is *ca.* $1.2 \times 10^{-3}\,\mathrm{s}^{-1}$ for $\Omega = 3.9\,\mathrm{rad\,s}^{-1}$ and $m = 6$, and it is independent of the sign of $T_b - T_a$.

(3) The vorticity gradient of the basic flow, as mentioned before, will also cause the waves to drift relative to the mean flow, and as previously discussed the drift velocities in the present experiments would be expected to be about $[-12\bar{u}/(b-a)^2] \times [(b-a)^2 l^2/(l^2 + 4(b-a)^2)\,\pi^2]$, i.e. typically of similar magnitude but opposite direction to $\bar{u}$. The sensitivity of the vorticity gradient to the shape of the velocity profiles means that changes in the profiles may confuse the effects of both changing Ω and sloping the lower boundary.

Table 21 B shows the differences between the drift rates with a sloping lower boundary and those in the corresponding experiments with a horizontal lower boundary. The majority of the

TABLE 21A. INVERSE WAVE DRIFT PERIODS ($\mathscr{T}^{-1} \times 10^3$) FOR SLOPING LOWER BOUNDARIES WITH A FREE UPPER SURFACE (LIQUID USED: WATER, $a = 3.80$ cm, $b = 8.43$ cm, $d = 12$ cm, $|T_b - T_a| \approx 10$ K)

	θ_1/deg									
	−36		−12		0		12		36	
Ω/rad s^{-1}	$T_a > T_b$	$T_a < T_b$	$T_a > T_b$	$T_a < T_b$	$T_a > T_b$	$T_a < T_b$	$T_a > T_b$	$T_a < T_b$	$T_a > T_b$	$T_a < T_b$
0.8	—	−6.67	4.55	−4.67	5.21	−3.77	5.95	−2.70	—	—
1.0	3.19	−5.62	4.24	−4.05	5.21	−4.27	5.05	−3.79	4.98	−1.36
1.4	3.12	−4.12	4.20	−3.40	4.39	−3.21	4.07	−2.90	5.38	−3.21
1.9	2.69	−5.05	4.17	−3.00	3.95	−2.82	3.02	−2.85	7.41	−3.17
2.3	2.26	—	2.67	−2.97	3.47	−3.16	3.80	−2.31	—	−2.87
2.7	1.64	—	2.17	−2.82	2.98	−2.28	3.97	−2.07	—	−2.85
3.1	—	—	1.98	—	2.56	−2.45	4.18	−1.70	—	—
3.4	—	—	1.47	—	2.31	−1.88	4.39	−1.39	—	—
3.9	—	—	1.10	—	1.89	−2.31	—	−1.08	—	—

TABLE 21B. CHANGES IN WAVE DRIFT RATES FOR SLOPING LOWER BOUNDARIES WITH A FREE UPPER SURFACE: THE DIFFERENCE BETWEEN THE EXPERIMENTAL DRIFT RATES ($\mathscr{T}^{-1} \times 10^{-3}$) WITH A SLOPING LOWER BOUNDARY, AND THOSE IN EXPERIMENTS FOR SIMILAR CONDITIONS BUT WITHOUT THE SLOPING LOWER BOUNDARY

	θ_1/deg							
	−36		−12		12		36	
Ω/rad s^{-1}	$T_a > T_b$	$T_a < T_b$	$T_a > T_b$	$T_a < T_b$	$T_a > T_b$	$T_a > T_b$	$T_a > T_b$	$T_a < T_b$
0.8	—	−2.10	−0.66	−0.90	0.74	1.07	—	—
1.0	−2.02	−1.35	−0.97	+0.22	−0.16	0.48	−0.23	2.91
1.4	−1.27	−0.91	−1.19	−0.19	−0.32	0.32	0.99	0.00
1.9	−1.26	−2.23	+0.23	−0.18	−0.93	−0.03	3.06	−0.35
2.3	−1.26	—	−0.80	+0.19	0.33	0.85	—	0.29
2.7	−1.34	—	−0.81	−0.54	0.99	0.21	—	−0.57
3.1	—	—	−0.58	—	1.62	0.75	—	—
3.4	—	—	−1.09	—	2.08	0.49	—	—
3.9	—	—	−0.79	—	—	1.23	—	—

changes in drift rate are in the same sense as expected from theory, i.e. same sign as θ_1, and as can be seen by comparing with the data in table 20 A, the size of the changes are similar to those in the corresponding rigid lid cases. However, the sign of the change in drift rate is not always the same as expected from theory, and as noted above, this poor agreement is probably due to changes in the slope of the isotherms and the shape of the velocity profiles. The presence in the free surface cases of a large mean flow and also a large β-effect due to shear, both of which may change when the boundaries are sloped or Ω is varied, precludes a meaningful comparison with theory unless the mean flow and vorticity gradient are measured directly.

(*e*) *Heat transfer measurements*

Heat transfer determinations were made more or less incidentally (as described in § 4 (*c*) (iv)) during the course of the experiments and gave the results described below.

(i) $\theta_1 = \theta_u$

Table 22 shows Nusselt numbers (§ 4 (*c*) (iv)) for rigid parallel upper and lower boundaries. In the $Q_1 = Q_u < 0$, $|\theta_1| = 36°$ case no fully developed waves occurred and the heat flow simply decreased with increasing Ω. A comparison of the other cases with the corresponding flow types

PHILOSOPHICAL TRANSACTIONS OF THE ROYAL SOCIETY A MATHEMATICAL, PHYSICAL & ENGINEERING SCIENCES

(table 11) shows that the heat transfer in the wave régime falls off with increasing Ω only when the irregular flow occurs. The changes in heat transfer produced by the slopes thus seem to be associated with the changes in the irregular transition.

TABLE 22. NUSSELT NUMBERS FOR RIGID PARALLEL UPPER AND LOWER BOUNDARIES (LIQUID USED: WATER, $a = 3.80$ cm, $b = 8.43$ cm, $d = 12$ cm, $|T_b - T_a| \approx 10$ K)

	$\lvert\theta_1\rvert$/deg × sgn Q_1							
		−12		0		12		
	−36							36
Ω/rad s^{-1}	$T_a > T_b$	$T_a > T_b$	$T_a < T_b$	$T_a > T_b$	$T_a < T_b$	$T_a > T_b$	$T_a < T_b$	$T_a < T_b$
0.5	8	8	9	9	9	8	9	9
†	–	7	8	8	8	7	8	8
1.0	7	9	9	9	8	8	9	8
1.4	4	8	8	8	9	7	8	8
1.9	4	7	7	8	8	7	8	8
2.3	3	6	7	8	8	7	7	8
2.7	2	4	6	8	8	7	8	8
3.1	2	4	5	7	8	7	8	8
3.5	1	4	5	7	8	7	8	7
3.9	1	4	5	6	7	7	7	8

† Measurement at the highest value of Ω for which symmetric flow occurred.

(ii) $\theta_1 = -\theta_u$

Table 23 shows Nusselt numbers for oppositely sloping upper and lower boundaries. For $T_a < T_b$ a small drop in heat transfer occurs at high Ω, but for $T_a > T_b$ a marked drop occurs. This change is not associated with the irregular or other flow type transitions, and it may be due to the combination of effects due to oppositely sloping boundaries and sloping geopotentials. The former $\partial d/\partial r \neq 0$ effect would be expected to produce a reduction in heat transfer, not only in correspondence with reduced growth rates in the linear theory, but also because of the observed limitation in the radial extent of the waves. The latter effect would by analogy with the parallel slope data, be expected to produce an increase in heat transfer for $T_b > T_a$ and a decrease for $T_b < T_a$.

(iii) $\theta_1 \neq 0$, $\theta_u = 0$

Table 24 shows Nusselt numbers for a sloping lower boundary with a rigid upper boundary. For $Q_1 < 0$ the heat transfer at high values of Ω is decreased. This is consistent with a reduction produced by the effect of $\partial d/\partial r \neq 0$ together with a $Q_1 = Q_u < 0$ effect. For $Q_1 > 0$ no change in the heat transfer occurs; this is in keeping with the effects of $\partial d/\partial r$ and $Q_1 = Q_u > 0$ acting in opposition.

Table 25 shows Nusselt numbers for sloping lower boundaries with a free upper surface. The Nusselt numbers for $T_a > T_b$ are seen to be generally less than with $T_a < T_b$ regardless of the sign of Q_1. This could be due to the effect of the sloping geopotentials. Apart from this change with the sign of $T_b - T_a$ the heat transfer at high Ω is seen to be markedly reduced for $Q_1 < 0$ and slightly reduced for $Q_1 > 0$. As with the case of a rigid horizontal upper lid these changes are consistent with a general decrease produced by $\partial d/\partial r \neq 0$ together with an increase or decrease according as $Q_1 \gtrless 0$.

The author wishes to thank Dr R. Hide, F.R.S. for his interest and support given to this work. This paper is published by permission of the Director-General of Meteorological Office.

TABLE 23. NUSSELT NUMBERS FOR OPPOSITELY SLOPING UPPER AND LOWER BOUNDARIES (LIQUID USED: WATER, $a = 3.80$ cm, $b = 8.43$ cm, DEPTH AT $r = \frac{1}{2}(a+b) = 12$ cm, $|T_b - T_a| \approx 10$ K)

	θ_1/deg					
	0		−12		−36	
Ω/rad s^{-1}	$T_a > T_b$	$T_a < T_b$	$T_a > T_b$	$T_a < T_b$	$T_a > T_b$	$T_a < T_b$
0.5	9	9	9	9	9	9
†	8	8	8	8	8	9
1.0	9	8	8	9	7	8
1.4	8	9	8	8	7	8
1.9	8	8	8	8	6	8
2.3	8	8	8	8	5	8
2.7	8	8	7	8	5	7
3.1	7	8	7	8	5	8
3.5	7	8	6	8	4	7
3.9	6	7	5	7	4	6

† Measurement at the highest value of Ω for which symmetric flow occurred.

TABLE 24. NUSSELT NUMBERS FOR SLOPING LOWER BOUNDARIES WITH A HORIZONTAL RIGID UPPER BOUNDARY (LIQUID USED: WATER, $a = 3.80$ cm, $b = 8.43$ cm, DEPTH AT $r = \frac{1}{2}(a+b) = 12$ cm, $|T_b - T_a| \approx 10$ K)

	$\lvert\theta_1\rvert$/deg × sgn Q_1					
			0			
	−36	−12			12	36
Ω/rad s^{-1}	$T_a > T_b$	$T_a > T_b$	$T_a > T_b$	$T_a < T_b$	$T_a < T_b$	$T_a < T_b$
0.5	9	9	9	9	9	9
†	8	8	8	8	9	9
1.0	9	9	9	8	9	9
1.4	9	9	8	8	9	8
1.9	7	8	8	8	9	8
2.3	6	8	8	8	8	8
2.7	5	7	8	8	8	8
3.1	4	6	7	8	8	8
3.5	4	5	7	8	8	8
3.9	3	4	6	7	7	8

† Measurement at the highest value of Ω for which symmetric flow occurred.

TABLE 25. NUSSELT NUMBERS FOR SLOPING LOWER BOUNDARIES WITH A FREE UPPER SURFACE (LIQUID USED: WATER: $a = 3.80$ cm, $b = 8.43$ cm, $d = 12$ cm, $|T_b - T_a| \approx 10$ K)

	$\lvert\theta_1\rvert$/deg × sgn Q_1									
	−36		−12		0		12		36	
Ω/rad s^{-1}	$T_a > T_b$	$T_a < T_b$	$T_a > T_b$	$T_a < T_b$	$T_a > T_b$	$T_a < T_b$	$T_a > T_b$	$T_a < T_b$	$T_a > T_b$	$T_a < T_b$
0.5	7	7	7	8	7	8	8	6	7	7
†	4	2	5	5	5	6	6	5	4	6
1.0	7	6	7	9	7	9	7	7	5	7
1.4	7	8	7	9	7	9	7	7	6	7
1.9	7	7	7	9	8	9	7	7	6	7
2.3	5	6	8	9	7	9	7	7	6	7
2.7	3	6	6	9	7	8	7	7	6	7
3.1	2	6	5	8	7	9	7	7	6	7
3.5	2	6	4	8	7	8	7	7	4	7
3.9	1	5	4	7	6	8	7	6	3	6

† Measurement at the highest value of Ω for which symmetric flow occurred.

PHILOSOPHICAL TRANSACTIONS OF THE ROYAL SOCIETY A MATHEMATICAL, PHYSICAL & ENGINEERING SCIENCES

References

Barcilon, V. 1964 Role of Ekman layers in the stability of the symmetric regime obtained in a rotating annulus. *J. atmos. Sci.* **21**, 291–299.

Blumsack, S. L. & Gierasch, P. J. 1972 Mars: The effects of topology on baroclinic instability. *J. atmos. Sci.* **29**, 1081–1089.

Bowden, M. & Eden, H. F. 1965 Thermal convection in a rotating fluid annulus: temperature, heat flow and flow field observations in the upper symmetric regime. *J. atmos. Sci.* **22**, 185–195.

Bretherton, F. P. 1966*a* Critical layer instability in baroclinic flows. *Q. Jl R. Met. Soc.* **92**, 325–334.

Bretherton, F. P. 1966*b* Baroclinic instability and the short wavelength cut-off in terms of potential vorticity. *Q. Jl R. Met. Soc.* **92**, 335–345.

Charney, J. G. & Stern, M. E. 1962 On the stability of internal baroclinic jets in a rotating atmosphere. *J. atmos. Sci.* **19**, 159–172.

Douglas, H. A., Hide, R. & Mason, P. J. 1973 An investigation of the structure of baroclinic waves using three-level streak photograph. *Q. Jl R. Met. Soc.* **98**, 247–263.

Douglas, H. A. & Mason, P. J. 1972 On the effect of changing the aspect ratio in a large differentially heated vertical rotating fluid annulus. *J. atmos. Sci.* **30**, 1124–1133.

Eady, E. T. 1949 Long waves and cyclone waves. *Tellus* **13**, 33–52.

Fowlis, W. W. & Hide, R. 1965 Thermal convection in a rotating fluid annulus: effect of viscosity on the transition between axisymmetric and non-axisymmetric flow regimes. *J. atmos. Sci.* **22**, 541–558.

Fultz, D. 1964 Research on hydrodynamic analogues of large-scale meteorological phenomena, final report to Air Force Cambridge Res. Lab. OAR, U.S.A.F. Bedford, Mass.

Fultz, D. & Kaylor, R. 1959 The propagation of frequency in experimental waves in a rotating annular ring. *Rossby Memorial Volume* (ed. B. Bolin). New York: Rockefeller Ins. Press.

Green, J. S. A. 1960 A problem in baroclinic stability. *Q. Jl R. Met. Soc.* **86**, 237–251.

Greenspan, H. P. 1968 *The theory of rotating fluids.* Cambridge University Press.

Hide, R. 1953 Some experiments on thermal convection in a rotating liquid. Ph.D. thesis, Cambridge University.

Hide, R. 1958 An experimental study of thermal convection in a rotating liquid. *Phil. Trans. R. Soc. Lond.* A **250**, 442–478.

Hide, R. 1967. On the vertical stability of a rotating fluid subject to a horizontal temperature gradient. *J. atmos. Sci.* **24**, 6–9.

Hide, R. 1969 Some laboratory experiments on free thermal convection in a rotating fluid subject to a horizontal temperature gradient and their relation to the theory of the global atmospheric circulation. In *The global circulation of the atmosphere* (ed. G. A. Corby), pp. 196–221. London: R. Met. Soc.

Hide, R. & Mason, P. J. 1975 Sloping convection in a rotating fluid: a review. *Adv. Phys.* **24**, 47–100.

Kaiser, J. A. C. 1969 Rotating deep annulus convection. Part 1. Thermal properties of the upper symmetric regime. *Tellus* **21**, 789–804.

Kaiser, J. A. C. 1970 Rotating deep annulus convection. Part 2. Wave instabilities vertical stratification and associated theories. *Tellus* **22**, 275–287.

Ketchum, C. B. 1972 An experimental study of baroclinic annulus waves at large Taylor number. *J. atmos. Sci.* **29**, 665–679.

Leovy, C. B. & Mintz, Y. 1969 A numerical general circulation experiment for the atmosphere of Mars. *J. atmos. Sci.* **26**, 1167–1190.

Lorenz, E. N. 1967 *The nature and theory of the general circulation of the atmosphere* (T.P. 115, no. 218). Geneva: W.M.O.

McIntyre, M. E. 1968 The axisymmetric convective regime for a rigidly bounded rotating annulus. *J. Fluid Mech.* **32**, 625–655.

Orlanski, I. & Cox, M. D. 1973 Baroclinic instability in ocean currents. *Geophys. Fluid Dynam.* **4**, 297–332.

Pedlosky, J. 1964 The stability of currents in the atmosphere and ocean. Parts I and II. *J. atmos. Sci.* **21**, 342–353.

Pfeffer, R. L. & Fowlis, W. W. 1968 Wave-dispersion in a rotating differentially heated cylindrical annulus of fluid. *J. atmos. Sci.* **25**, 361–371.

Pfeffer, R. L., Fowlis, W. W., Fein, J. & Buckley, J. 1970 Experimental determinations of the transition between the symmetrical and wave regimes in a rotating differentially heated annulus of fluid. *Pure app. Geophys.* **81**, 263–271.

Schulman, E. E. 1967 The baroclinic instability of a mid-ocean circulation. *Tellus* **19**, 292–305.

Smith, A. R. 1958 The effect of rotation on the flow of a baroclinic liquid. Ph.D. thesis, Cambridge University.

Veronis, G. 1963 On the approximations involved in transforming the equations of motion from a spherical surface to the β-plane. I. Barotropic Systems. II. Baroclinic Systems. *J. marine Res.* **21**, I, 110–124; II, 199–204.

Ward, F. 1965 The general circulation of the solar atmosphere and the maintenance of the equatorial acceleration. *Astrophys. J.* **141**, 534–547.

Williams, G. P. 1967 Thermal convection in a rotating fluid annulus. I. The basic axisymmetric flow. *J. atmos. Sci.* **24**, 144–161.

PHILOSOPHICAL TRANSACTIONS OF THE ROYAL SOCIETY A MATHEMATICAL, PHYSICAL & ENGINEERING SCIENCES